Journal of Volcanology and Geothermal Research 349 (2018) 31–46

Contents lists available at ScienceDirect

Journal of Volcanology and Geothermal Research

journal homepage: www.elsevier.com/locate/jvolgeores

Petrological constraints on the high-Mg basalts from Capo Marargiu (Sardinia, Italy): Evidence of cryptic amphibole fractionation in polybaric environments

Vanni Tecchiato [a,*], Mario Gaeta [a], Silvio Mollo [a], Piergiorgio Scarlato [b], Olivier Bachmann [c], Cristina Perinelli [a]

[a] Dipartimento di Scienze della Terra, Sapienza-Università di Roma, Piazzale Aldo Moro 5, 00185 Roma, Italy
[b] Istituto Nazionale di Geofisica e Vulcanologia, Via di Vigna Murata 605, 00143 Roma, Italy
[c] Institute of Geochemistry and Petrology, ETH Zürich, Clausiusstrasse 25, 8092 Zurich, Switzerland

ARTICLE INFO

Article history:
Received 8 May 2017
Received in revised form 30 August 2017
Accepted 17 September 2017
Available online 22 September 2017

Keywords:
Crystal-rich enclaves
High-Mg basalts
Cryptic amphibole fractionation
Crystal entrainment
Polybaric crystallisation
Sardinia magmatism

ABSTRACT

This study deals with the textural and compositional characteristics of the calc-alkaline stratigraphic sequence from Capo Marargiu Volcanic District (CMVD; Sardinia island, Italy). The area is dominated by basaltic to intermediate hypabyssal (dikes and sills) and volcanic rocks (lava flows and pyroclastic deposits) emplaced during the Oligo-Miocene orogenic magmatism of Sardinia. Interestingly, a basaltic andesitic dome hosts dark-grey, crystal-rich enclaves containing up ~50% of millimetre- to centimetre-sized clinopyroxene and amphibole crystals. This mineral assemblage is in equilibrium with a high-Mg basalt recognised as the parental magma of the entire stratigraphic succession at CMVD. Analogously, centimetre-sized clots of medium- and coarse-grained amphibole + plagioclase crystals are entrapped in andesitic dikes that ultimately intrude the stratigraphic sequence. Amphibole-plagioclase cosaturation occurs at equilibrium with a differentiated basaltic andesite. Major and trace element modelling indicates that the evolutionary path of magma is controlled by a two-step process driven by early olivine + clinopyroxene and late amphibole + plagioclase fractionation. In this context, enclaves represent parts of a cumulate horizon segregated at the early stage of differentiation of the precursory high-Mg basalt. This is denoted by i) resorption effects and sharp transitions between Mg-rich and Mg-poor clinopyroxenes, indicative of pervasive dissolution phenomena followed by crystal re-equilibration and overgrowth, and ii) reaction minerals found in amphibole coronas formed at the interface with more differentiated melts infiltrating within the cumulate horizon, and carrying the crystal-rich material with them upon eruption. Coherently, the mineral chemistry and phase relations of enclaves indicate crystallisation in a high-temperature, high-pressure environment under water-rich conditions. On the other hand, the upward migration and subsequent fractionation of the residual basaltic andesite in a shallower, colder, and hydrous region of the CMVD plumbing system lead to the formation of the amphibole-plagioclase crystal clots finally entrained by the andesitic dikes. Indeed, phenocrysts from these more evolved products record the final crystallisation path of magma during ascent towards the surface. Magma decompression and volatile loss cause the formation of amphibole reaction coronas and the crystallisation of a more sodic plagioclase in equilibrium with basaltic andesitic to andesitic melts. The bulk-rock geochemical signature of these products testifies to open-system, polybaric magma dynamics, accounting for variable degrees of crustal assimilation of the Hercynian basement of Sardinia.

1. Introduction

Differentiation of hydrous, mantle-derived basalts is a fundamental process to generate intermediate to SiO_2-rich products commonly erupted in continental and island arc settings. The stratigraphic architecture of the crust encountered by primary magma *en route* to surface dictates how and where differentiation acts. The most important density trap that primarily constrains cooling and crystallisation of primitive magmas is likely located at the mantle-crust transition (i.e., Mohorovičić discontinuity), where high pressure conditions may prevent water loss, thus promoting amphibole formation. Calc-alkaline melts extracted from such deep-seated crystal mushes typically inherit the geochemical signature of amphibole fractionation (i.e., trends of decreasing Dy/Yb and increasing La/Yb with SiO_2), reflecting leverage of this mineral on the behaviour of both trace (Rare Earth Elements) and major (SiO_2) elements during earlier stages of magmatic evolution (Davidson et al., 2007). Despite the intriguing paucity of this mineral as a major constituent in arc lavas (e.g., Tilley, 1950), a number of experimental works (Alonso-Perez et al., 2009; Cawthorn and O'Hara, 1976; Foden and Green, 1992; Green and Ringwood, 1968; Grove et al., 2003; Gust and Perfit, 1987; Holloway and Burnham, 1972; Melekhova et al., 2015;

* Corresponding author.
E-mail address: vanni.tecchiato@uniroma1.it (V. Tecchiato).

https://doi.org/10.1016/j.jvolgeores.2017.09.007
0377-0273/

Pichavant and Macdonald, 2007) provide significant evidence that such a process "cryptically" occurs at the roots of volcanic arcs. Accordingly, large volumes of unerupted amphibole gabbros, diorites, tonalites, and amphibolites outcrop in exhumed deep crustal suites derived from subduction environments (Abd El-Rahman et al., 2012; Larocque and Canil, 2010; Best, 1975; Davidson et al., 2007; DeBari and Coleman, 1989; Dessimoz et al., 2012; Ducea and Saleeby, 1996; Lewis, 1973; Smith, 2014; Stamper et al., 2014; Yamamoto, 1984). Alternatively, portions of these plutonic rocks or individual amphibole megacrysts entrapped within erupted products provide textural and compositional information to qualitatively and quantitatively infer magmatic processes and intensive parameters of crystallisation at depth (Bachmann and Dungan, 2002; Chadwick et al., 2013; De De Angelis et al., 2013; Shane and Smith, 2013; Turner et al., 2013).

Prior to eruption, buoyant high Al-basaltic, basaltic andesitic and andesitic melts (Melekhova et al., 2015; Pichavant and Macdonald, 2007) extracted from lower crustal mushes and ascending through the crust have more than one opportunity to be further stopped at variable depths, depending on how their physical properties differ from those of country rocks (Gudmundsson, 2011). This can lead to complexly structured plumbing systems built by multiple magma chambers and reservoirs more or less interconnected to each other (e.g., Elsworth et al., 2008). In the shallower portions of these systems, the intermediate melts are subjected to additional steps of differentiation towards more evolved compositions (Lipman et al., 1978; Foden and Green, 1992; Dufek and Bachmann, 2010; Bachmann and Huber, 2016; Cashman et al., 2017). Residual cumulates fractionated at shallow levels are typically more siliceous than those segregated at higher depths, providing modal and chemical heterogeneities throughout the entire crustal cumulate pile (Dufek and Bachmann, 2010). Identifying the discrete mineral assemblages determining the multistage physicochemical evolution of arc series is fundamental for a correct interpretation of magmatic processes.

The Capo Marargiu Volcanic District (i.e., CMVD; Sardinia island, Italy) represents an interesting case of amphibole-driven polybaric differentiation from near-primary high-Mg basaltic to andesitic products. In this contribution, mineral textures and compositions of crystal-rich enclaves (up ~50% of millimetre- to centimetre-sized clinopyroxene and amphibole crystals) and amphibole-plagioclase crystal clots hosted in intermediate domes and dikes are used to (1) model major and trace element bulk-rock data, (2) estimate magma crystallisation conditions by comparing thermometric, barometric, hygrometric, and oxygen barometric data with phase relation diagrams.

2. Geological setting

Sardinia is one of the largest islands in the central-western Mediterranean region, at the subduction-collisional boundary between the European and the westward-subducted Ionian and Adria plates. In this geodynamic context, the Apennine-Maghrebide fold-and-thrust belt migrated from eastward to southward from the late Cretaceous (~80 Ma) and during the Cenozoic (Carminati et al., 2012; Lustrino et al., 2004, 2009). Afterwards, this migration was followed by back-arc stretching and boudinage of the European upper plate, driving the formation of a series of V-shaped basins and to the isolation of lithospheric ribbons in the middle of Central-Western Mediterranean area (Carminati et al., 2012, and references therein). Sardinia represents one of these lithospheric ribbons rotated ~55–60° counter-clockwise away from the European paleo-margin during the Late Oligocene-Early Miocene (Cherchi et al., 2008; Dieni et al., 2008, and references therein). The rotation was the result of an initial stage of rifting and subsequent drifting, also accompanied by the widespread production of magmas with subduction fingerprint (Lustrino et al., 2013).

The orogenic magmatism ranged from ~38 to ~13 Ma (Late Eocene-Middle Miocene) with a productivity peak at ~22–18 Ma (Lustrino et al., 2009). Igneous rocks were almost exclusively erupted in a graben structure crossing the island from north to south, called the Fossa Sarda (Sardinian Trough). In particular, intense volcanism interested the Logudoro-Bosano domain (north-western Sardinia), where four eruptive sequences were identified: basal (or lower) andesitic series, lower ignimbritic series, upper andesitic series, and upper ignimbritic series (Coulon and Baque, 1973; Coulon et al., 1978; Deriu, 1964). The overall compositions of rocks in the Logudoro-Bosano domain span from basalt to rhyolite. The most primitive terms are high-Mg basalts from the Montresta locality, ~10 km northeast of Capo Marargiu area (Morra et al., 1997). From a geochemical point of view, the Montresta rocks evolve towards calc-alkaline basalts and high-K calc-alkaline basaltic andesites. The incompatible trace element variation denotes the typical subduction-related geochemical characteristics of arc magmas (e.g., Avanzinelli et al., 2009; Duggen et al., 2005; Lustrino et al., 2011). The faintly LREE-enriched and HREE-flattened chondrite-normalised patterns point to a spinel-bearing mantle source (Brotzu et al., 1997b; Franciosi et al., 2003; Lustrino et al., 2009; Morra et al., 1997). An important feature of the Logudoro–Bosano rocks is also represented by the variation of Nd—Sr isotopes relative to SiO_2, interpreted as either the effect of magma-crust interaction processes at shallow-levels (Morra et al., 1997; Franciosi et al., 2003; Lustrino et al., 2013), or the involvement of terrigenous subducted sediments/fluids in the mantle source (Franciosi et al., 2003; Lustrino et al., 2013). The CMVD is located at ~10 km south-westward of Montresta (Fig. 1a). Lecca et al. (1997) categorised the stratigraphic succession in andesitic domes, andesitic autoclastic and blocky lava flows (i.e., lower andesitic series), dikes, and welded ignimbrites. Geochronological studies conducted with the K—Ar method provided ages between 24 ± 1.2 Ma (Montigny et al., 1981) and 17.3–17.7 ± 0.4 Ma (Coulon et al., 1974) from the bottom (andesitic domes) to the top (welded ignimbrites) of the Oligo-Miocene stratigraphic succession. The high-Mg basalts at Montresta have K—Ar ages of 18.5 ± 1.2 Ma (Montigny et al., 1981) comparable to those of products at the CMVD (Coulon et al., 1974; Montigny et al., 1981). At the end of magmatism, the volcanic edifice was eroded exposing hypabyssal and volcanic rocks from the shallowest part of the plumbing system.

3. Field characters and rock sampling

The fieldwork targeted the geological formations of the Capo Marargiu area previously described by other authors (cf. Deriu, 1964; Lecca et al., 1997). Lava domes are the main products, being usually in lateral contact with volcanic breccias. Locally, lava flows or stratified pyroclastic deposits are found. Dikes and sills are abundant and intrude both the domes and the volcanic breccias. All these rocks belong to the first (i.e., lower andesitic series) eruptive sequence described by Coulon et al. (1978). The shift from older volcanic to younger hypabyssal products testifies to the accretion of the volcanic edifice as a result of multiple eruptive episodes. The sampling focused on the coast of Cala Bernardu (Fig. 1b), where a cliff exposed the inner part of an andesitic dome hosting abundant crystal-rich enclaves (Fig. 1c). The dome appears as a yellowish, porphyritic rock with ~15% of phenocrysts. In contrast, the dark-grey enclaves are centimetre-to-metre-sized rounded blocks with ~50% of coarse-grained crystals (Fig. 1c). Some portions of the dome are also slightly darker and richer in crystals due to enclave disaggregation in the surrounding magma. Dikes intruding the andesitic dome are characterised by radial orientation variable thickness (0.3–2 m), and the occurrence of centimetre-sized clots of medium- and coarse-grained amphibole + plagioclase crystals.

For the purpose of this study, a total amount of twenty-eight rocks were collected and investigated for mineral and bulk-rock major elements (see Appendix A for analytical methods). These rocks comprise seven samples for the enclaves, ten samples for the host dome, six samples for dikes, and five samples for the crystal clots (Table 1B).

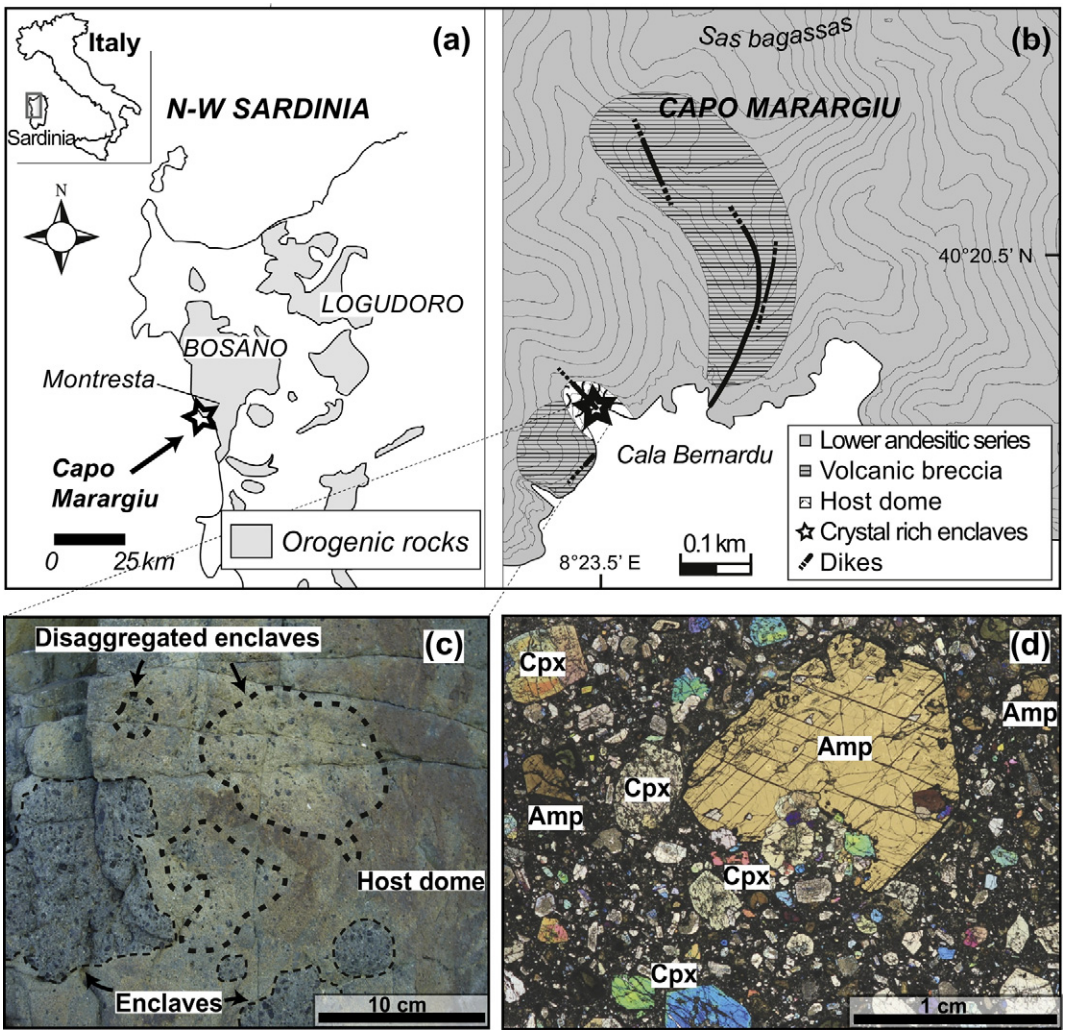

Fig. 1. Schematic maps showing the Capo Marargiu Volcanic District (i.e., CMVD) located at about 10 km south-westward of Montresta (Sardinia, Italy) (a) and the sampling area of the volcanic dome on the coast of Cala Bernardu (b). The studied rocks are enclaves, host dome, dikes and crystal clots. The dome appears as a yellowish, porphyritic rock, whereas the dark-grey enclaves are centimetre-to-metre-sized rounded blocks (c). Some portions of the dome are also enriched in crystals produced by enclave disaggregation in the surrounding magma (c). The enclaves are crystal-rich, porphyritic rocks containing ~40–50% of coarse-grained clinopyroxene + amphibole + plagioclase + olivine + titanomagnetite/ilmenite ± Cr-spinel (d). Clinopyroxene (i.e., Cpx) and amphibole (i.e., Amp) are the most abundant minerals.

4. Petrography and mineral chemistry

In this section, each rock type (i.e., enclaves, host dome, dikes, crystal clots) is described combining textural observations and mineral chemistry data (Figs. 1–4). Comparisons are also provided to point out the compositional difference of the most abundant minerals (i.e., amphibole, plagioclase, and clinopyroxene) among the studied products (Figs. 3–4).

4.1. Enclaves

Enclaves are crystal-rich, porphyritic rocks (Fig. 1d) containing ~40–50% of coarse-grained (not univocally phenocrysts) clinopyroxene + amphibole + plagioclase + olivine + titanomagnetite/ilmenite ± Cr-spinel (in order of abundance). The millimetre-to-centimetre-sized minerals are dispersed in a microcrystalline groundmass of plagioclase + clinopyroxene + titanomagnetite ± low-Ca pyroxene. The most striking textural and compositional characteristics consist of the occurrence of two types of clinopyroxenes (Fig. 2):

- Type 1 clinopyroxenes appear as large crystal cores (> 1 mm) showing intense fracturing and disequilibrium dissolution features (Fig. 2a and b), i.e., sub-rounded edges, spongy cellular textures, and patchy zoning. The crystal composition is diopsidic (Wo_{41-48}-En_{40-50}-Fs_{5-14}; Morimoto, 1988) with Mg-number [Mg# = 100 · Mg/(Mg + Fe_{tot})] ranging from 75 to 91 (Table 2B). Al_{tot} is negatively correlated with Mg# (Fig. 2d). Patchy zoning along cracks (Fig. 2a) and around the voids of spongy crystals (Fig. 2b) results when Type 1 clinopyroxenes are in the process of reaction with the surrounding melt feeding the growth of Type 2 clinopyroxenes;
- Type 2 clinopyroxenes occur either as thick (0.1–0.5 mm) crystal rims around Type 1 cores entrapping Usp_{20-40} titanomagnetite + An_{88-93} plagioclase ± altered olivine (Fig. 2a), or as millimetre-sized glomerocrysts together with the same plagioclases and titanomagnetites (Fig. 2c). The clinopyroxene composition is augitic (Wo_{41-45}-En_{42-45}-Fs_{12-16}; Table 2B) with $Mg\#_{72-79}$ lower than that measured for Type 1. The concentration of Al_{tot} is generally low (0.211–0.230 apfu) and decoupled with respect to Mg# (Fig. 2d). Clinopyroxene microlites (≤30 μm) show the most evolved compositions, i.e., $Mg\#_{70-76}$ and Al_{tot} contents in the range of 0.057–0.208 apfu (Fig. 2d).

Amphibole consists of large crystals (from 1 to 20 mm in size; Fig. 3a) with dark, fine-grained (<5 μm) reaction rims including groundmass minerals of clinopyroxene + plagioclase + titanomagnetite/ilmenite ± low-Ca pyroxene (Fig. 3b and c). These crystal rims may also develop on amphibole cores with spongy cellular textures

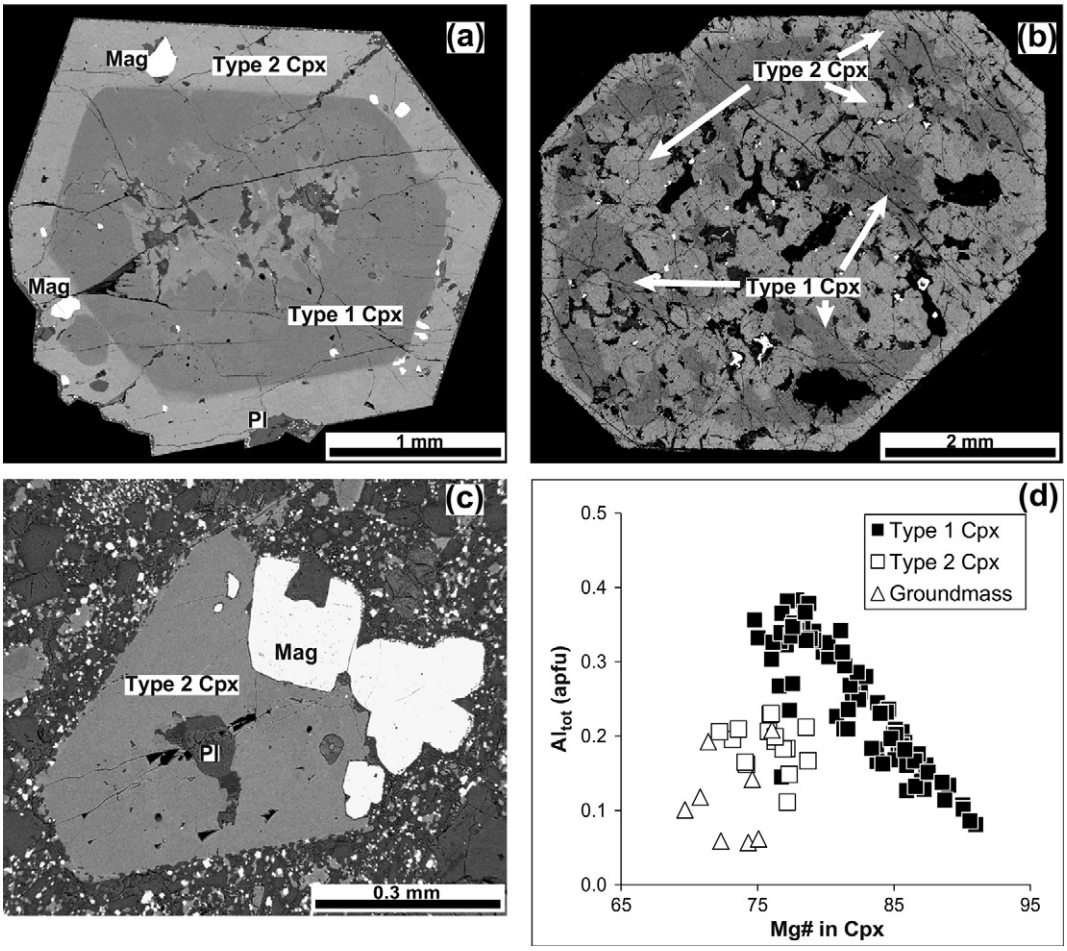

Fig. 2. Textural characteristics of Type 1 and Type 2 clinopyroxenes from enclaves. Type 2 crystals are observed to overgrow on Type 1 clinopyroxenes (a). Dissolution reaction phenomena form spongy cellular texture and patchy zoning (b). Heavy chemical species (more primitive portions of Type 1) backscatter electrons better than light elements (more evolved portions of Type 2). Type 2 grains occur also as millimetre-sized glomerocrysts together with plagioclase and titanomagnetite (c). Type 1 crystals are generally more primitive than Type 2 clinopyroxenes and groundmass microlites (d). Error bars are within the symbols.

(Fig. 3a) and the thickness of the reaction boundary is highly variable from 0.02 to 0.5 mm. According to the classification scheme of Leake et al. (1997), the composition of amphibole is magnesiohastingsite (Table 3B). The $Mg\#_{68-76}$ is also positively correlated with Al_{tot} (Fig. 3d), but most of the analytical dataset is restricted to a nearly constant value of Al_{tot} between 2.6 and 2.8 apfu. Generally, amphibole crystals including An_{72-93} plagioclase show the lowest values of Mg# (between 68 and 71) and Al_{tot} (between 2.2 and 2.6 apfu).

Plagioclase is found as either large, isolated crystals of a few millimetres in size, or small crystals entrapped in Type 2 clinopyroxenes (Fig. 2c) and, less frequently, in $Mg\#_{68-71}$ amphiboles. Plagioclase is characterised by continuous normal zoning with anorthite (An_{78-94}) content variable from core-to-rim (Fig. 4a; Table 4B). Microlites are generally less calcic showing An_{72-88} compositions.

Olivine occurs as millimetre-sized crystals typically altered to secondary iddingsite and, for this reason, it is rarely analysable for mineral texture and composition. Normally zoned crystals show primitive cores characterised by forsterite (Fo) contents from 84 to 87, whereas the rims are more evolved with Fo_{75-79} (Table 5B). The concentration of CaO (≤0.22 wt%) is also inversely proportional to the forsterite component.

Titanomagnetite grains have maximum size of 0.5 mm and are frequently associated with Type 2 clinopyroxenes. The ulvöspinel (Usp) content ranges between 3 and 42 (Table 6B).

Low-Ca pyroxene microlites are rare, showing Wo_{2-7}-En_{65-74}-Fs_{24-35} compositions and $Mg\#_{67-76}$ (Table 2B).

Cr-spinel has been found only in one sample (i.e., CM42) and in association with the most primitive olivine (Fo_{87}). The chemical composition is Usp_{38} with Cr-number [Cr# = Cr/(Cr + Al)] of 0.58.

4.2. Host dome

The host dome is porphyritic with plagioclase and clinopyroxene phenocrysts (≤15%) clashing abruptly with the plagioclase + clinopyroxene + low-Ca pyroxene + titanomagnetite groundmass.

Millimetre-sized (≤3 mm) plagioclase phenocrysts occur either as single, isolated crystals or as monomineralic glomerocrysts. Phenocrysts are characterised by normal zoning with An_{75-95} cores that are sharply overgrown by thin (20–30 μm) An_{45-71} rims (Fig. 4a; Table 4B). Plagioclase microlites (≤0.05 mm) are euhedral and unzoned, showing An_{49-72} compositions comparable to those of plagioclase rims. In spite of the extreme phenocryst-to-microlite variability of anorthite content (i.e., difference of ~45 mol% of An), the FeO concentration of plagioclase stays almost constant around an average of ~0.6 wt%.

Clinopyroxene phenocrysts are rare and frequently associated with titanomagnetite. The crystal size (≤1 mm) is usually smaller than that of plagioclase. Both clinopyroxene phenocrysts (Wo_{23-44}-En_{41-51}-Fs_{13-26}) and microlites (Wo_{36-42}-En_{38-44}-Fs_{15-20}) are augites showing almost homogeneous compositions with $Mg\#_{64-77}$ and Al_{tot} contents from 0.037 to 0.218 apfu (Fig. 4b).

Low-Ca pyroxene is more abundant with respect to enclaves and its chemistry is Wo_{1-14}-En_{54-68}-Fs_{30-39} and $Mg\#_{60-69}$ (Table 2B).

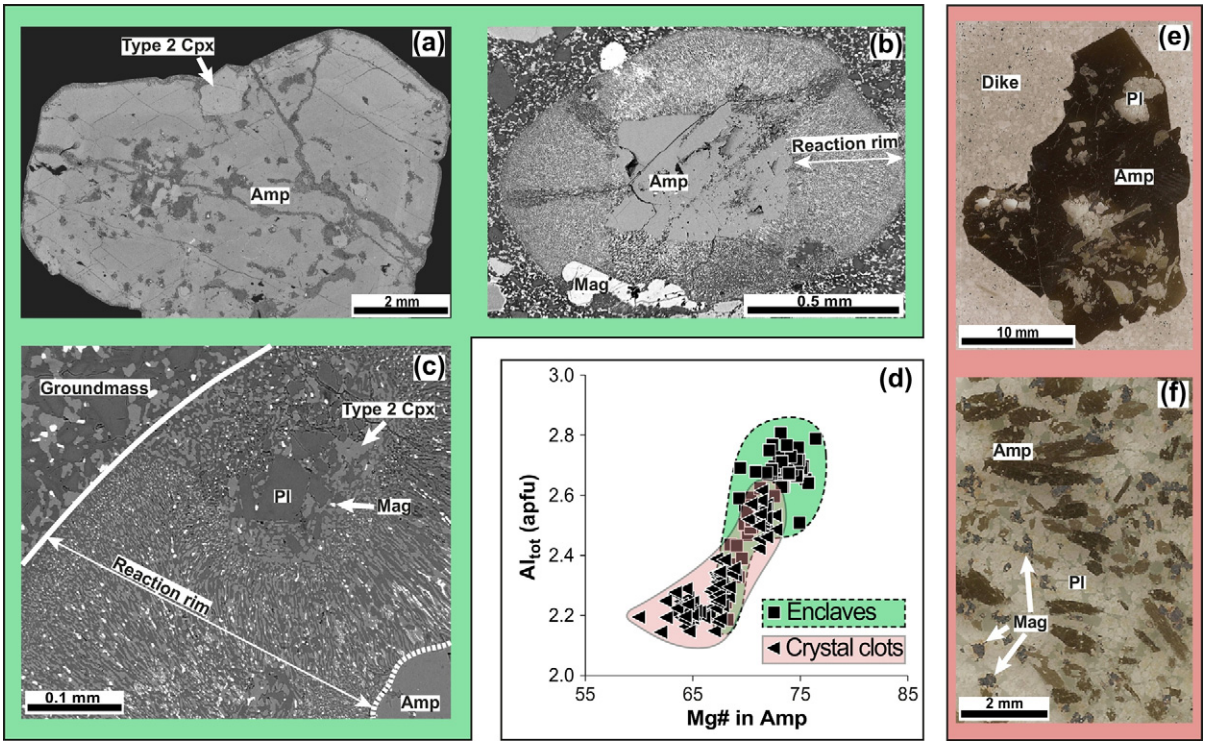

Fig. 3. Textural characteristics of amphiboles from enclaves and crystal clots. Amphibole are millimetre-to-centimetre sized crystals characterised by spongy cellular texture (a) with fine-grained reaction rims including groundmass minerals of clinopyroxene + plagioclase + titanomagnetite/ilmenite ± low-Ca pyroxene (b and c). The composition of amphibole from enclaves is magnesiohastingsite and most of the analytical dataset is restricted to a nearly constant value of Al_{tot} between 2.6 and 2.8 apfu (d). These data partially overlap with those of amphibole from crystal clots, which however are mostly evolved and restricted to values of Al_{tot} between 2.2 and 2.4 apfu (error bars within the symbols). Coarse-grained clots are characterised by centimetre-sized, texturally homogeneous amphibole crystals (e). Plagioclase is scarce in the coarse-grained clots (e), whereas its abundance increases in the medium-grained samples up to levels comparable to the amphibole contents (f).

Titanomagnetite occurs as small, $Usp_{10–50}$ crystals (Table 6B).

Two samples (i.e., TG21C and B6) show an apparent high crystallinity (≤35%) caused by the mechanical disaggregation of the enclaves into the host dome. Clinopyroxene and amphibole xenocrysts are the most abundant minerals with textural evidence of disequilibrium with the host magma, and compositions identical to those documented for the enclaves. Clinopyroxene xenocrysts exhibit corroded $Wo_{44–48}$-$En_{40–51}$-$Fs_{4–15}$ cores with $Mg\#_{71–93}$ and low Al_{tot} contents ranging from 0.062 to 0.383 apfu (Fig. 4b). These diopsidic cores are marked by the overgrowth of idiomorphic augitic rims with compositions ($Wo_{39–47}$-$En_{39–46}$-$Fs_{10–20}$, $Mg\#_{68–77}$, and Al_{tot} from 0.056 to 0.251 apfu) comparable to those of microlites in the groundmass (Fig. 4b). Amphiboles show thick (≤0.5 mm) reaction rims due to the occurrence of coarse-grained (0.05–0.1 mm) mineral associations of clinopyroxene + plagioclase + ilmenite. The composition of amphibole is prevalently magnesiohastingsite with $Mg\#_{69–74}$ and Al_{tot} contents ranging from 2.490 to 2.726 apfu (Table 3B).

4.3. Dikes

Dike samples are fine-grained (≤0.5 mm), weakly porphyritic (<10% phenocrysts), and glomeroporphyritic rocks. The paragenesis consists

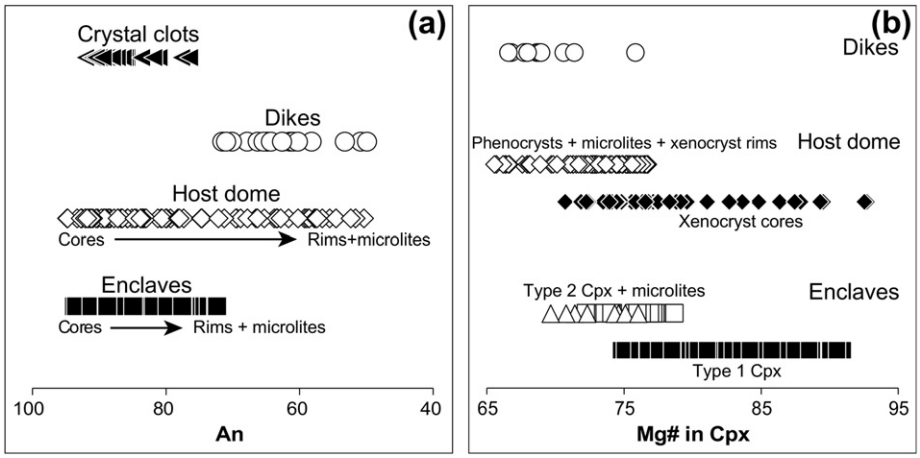

Fig. 4. Compositional variations of plagioclase (a) and clinopyroxene (b) crystals from the studied rocks (error bars within the symbols). An is anorthite in plagioclase. Mg# is Mg-number [i.e., 100 · Mg/(Mg + Fe_{tot})] in clinopyroxene.

of plagioclase + clinopyroxene + titanomagnetite, either as single phenocrysts or polymineralic glomerocrysts. The same mineral assemblage is found in the groundmass.

Plagioclase composition is relatively sodic, being $An_{50–71}$ (Fig. 4a). Interestingly, its composition overlaps with that measured for both phenocryst rims and microlites from host dome. Clinopyroxene is augite ($Wo_{40–44}$-$En_{39–43}$-$Fs_{14–20}$) with $Mg\#_{67–76}$ and low Al_{tot} concentrations (0.064–0.163 apfu), as observed for the most evolved microlites from enclaves and phenocrysts from host dome (Fig. 4b).

Titanomagnetite is $Usp_{31–50}$ (Table 6B).

The occurrence of secondary minerals testifies to post-magmatic hydrothermal alteration. Tiny crystals of calcite, chlorite, and quartz, are found to replace the small igneous crystals (likely pyroxenes) or filling voids and fractures.

4.4. Crystal clots

Medium-grained (millimetre-sized) to coarse-grained (centimetre-sized) gabbroic crystal clots of amphibole + plagioclase + titanomagnetite are hosted in dike rocks (Fig. 3).

Amphibole in the coarse-grained clots is subhedral to euhedral with size up 3 cm (Fig. 3e). Centimetre-sized amphiboles occur either as texturally homogeneous crystals (Fig. 3e), or as oikocrysts including $An_{77–92}$ plagioclase + $Usp_{15–58}$ titanomagnetite. Dark, thin (≤0.1 mm) reaction rims of micron-sized clinopyroxene + plagioclase + ilmenite + low-Ca pyroxene develop at the edges of amphibole crystals and in direct contact with the groundmass.

The composition of amphibole is magnesiohastingsite, but some crystals are also tschermakitic pargasite (Table 3B). The $Mg\#_{60–73}$ is positively correlated with Al_{tot}, although the majority of data are restricted to Al_{tot} between 2.2 and 2.4 apfu (Fig. 3d). Notably, the centimetre-sized amphiboles show the most primitive compositions ($Mg\#_{70–73}$) and contain scarce mineral inclusions (Fig. 3e).

Plagioclase is subhedral with maximum size in the order of a few millimetres. The overall compositional variation is $An_{77–92}$. (Fig. 4a). Plagioclase abundance is exiguous in the coarse-grained clots (Fig. 3e), whereas it increases in the medium-grained samples up to levels comparable to the amphibole contents (Fig. 3f).

Small titanomagnetite crystals are $Usp_{15–58}$ and their compositions resemble those from the host dome (Table 6B).

5. Bulk-rock geochemistry

Bulk-rock data from this study are reported in Table 7B, also in comparison with the calc-alkaline basalts and high-K calc-alkaline basaltic andesites from Montresta (cf. Morra et al., 1997). According to the TAS (total alkali vs. silica) classification scheme of Le Le Bas et al. (1986), rock samples are basalts, basaltic andesites, and andesites (Fig. 5) whose geochemical affinity shifts from calc-alkaline to high-K calc-alkaline (cf. Peccerillo and Taylor, 1976). Enclaves are high-Mg basalts (9.3–10.7 wt% MgO and 46.0–48.6 wt% SiO_2), whereas the host dome samples are basalts and basaltic andesites (3.8–6.5 wt% MgO and 49.8–54.2 wt% SiO_2). The most primitive host dome compositions (6.4–6.5 wt% MgO and 49.8–52.4 wt% SiO_2) are found for the high crystallinity samples (i.e., TG21C and B6) due to the mechanical disaggregation of enclaves into the basaltic andesitic host magma. Rationally, these compositions are outliers to the typical host dome chemistry, and their use is not contemplated for the following calculations (see below). Dikes are basaltic andesites to andesites (2.5–5.1 wt% MgO and 52.9–60.9 wt% SiO_2), except for the basaltic sample CM27 (4.9 wt% MgO and 50.5 wt% SiO_2) whose composition is affected by entrainment of abundant crystal clots.

From enclaves to host dome to dikes, SiO_2 (Fig. 6a) and Al_2O_3 (Fig. 6b) are negatively correlated with MgO. Conversely, Fe_2O_3 (Fig. 6c) and CaO (Fig. 6d) monotonically decrease with decreasing MgO, showing kinks at ~4–5 wt% MgO. Notably, the concentration of Al_2O_3 slightly decreases in the more evolved andesites (≤4 wt% MgO) due to the crystallisation of plagioclase (Fig. 6b).

Chondrite-normalised patterns (Fig. 7a) of Rare Earth Elements (REE) show enrichments in Light Rare Earth Elements (LREE) relative to Heavy Rare Earth Elements (HREE). From enclaves to host dome to dikes, the La_N/Lu_N ratio increases from 3.1 to 6.5 (Table 7B). A more pronounced negative Eu anomaly is observed from primitive to more evolved rock types (Fig. 7a), whereas the Eu/Eu* ratio (i.e., $Eu_N/[\sqrt{(Sm_N)} \times \sqrt{(Gd_N)}]$) decreases from 1.06 to 0.78.

Primitive mantle-normalised trace element patterns (Fig. 7b) show the typical geochemical characteristic of subduction-related rocks, consisting of variable enrichments in Large Ion Lithophile Elements (LILE; i.e., K, Rb, Sr, Ba, U, Th, and Pb) coupled with remarkable negative anomalies for some High Field Strength Elements (HFSE; i.e., Nb and Ta). Substantial enrichments of incompatible trace elements are also observed from enclaves to dikes, except for Cs and Ti in dike rocks (Fig. 7b).

6. Discussion

6.1. Constraining the parental magma composition

By comparing the compositions of Mg-rich enclaves and the most primitive basalts from Sardinia, it is possible to identify the parental magma feeding the volcanic activity at CMVD. High-Mg basaltic rocks (MgO > 7 wt%) are quite rare in the Sardinian orogenic area, exposed only in a few localities: i) Montresta and Capo Marargiu (i.e., CMVD) from the northern part of the island, and ii) Capo Frasca and Marmilla (cf. Lustrino et al., 2013), Arcuentu (cf. Brotzu et al., 1997b), and Villanovaforru (cf. Mattioli et al., 2000), from the southern part. Concerning the Montresta stratigraphic succession, Morra et al. (1997) categorised two types of basaltic products on the basis of their major element analyses (Fig. 5): 1) near-primary, mantle-derived high-Mg basalts (HMB), and 2) more differentiated high-Al basalts (HAB). In this context, enclaves, host dome, and dikes from this study are compositionally very similar to HMB, HAB, and basaltic andesites (BA) from Montresta (Figs. 5 and 6). However, Cr (186–338 ppm) and Ni (26–133 ppm) concentrations of enclaves are significantly lower than those (Cr = 186–739 ppm and Ni = 47–226 ppm) measured for HMB products. In turn, Sc (74–81 ppm) and V (457–470 ppm) contents of the former are 1.5–2 times higher than those (Sc = 42–51 ppm and V = 261–318 ppm) found in the latter. Chondrite-normalised REE and primordial mantle-normalised trace element patterns also denote compositional discrepancies between HMB products from Montresta and enclaves (Fig. 7). HMB products are clearly the most primitive rocks of the entire stratigraphic

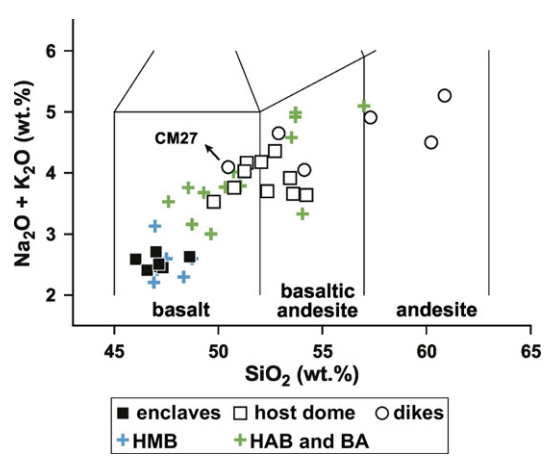

Fig. 5. Bulk-rock compositions of products from the CMVD are plotted in the TAS (total alkali vs. silica) diagram of Le Bas et al. (1986). Data from this study are also compared with the Montresta compositions reported by Morra et al. (1997), i.e., high-Mg basalts (HMB), more differentiated high-Al basalts (HAB), and basaltic andesites (BA). Error bars are within the symbols.

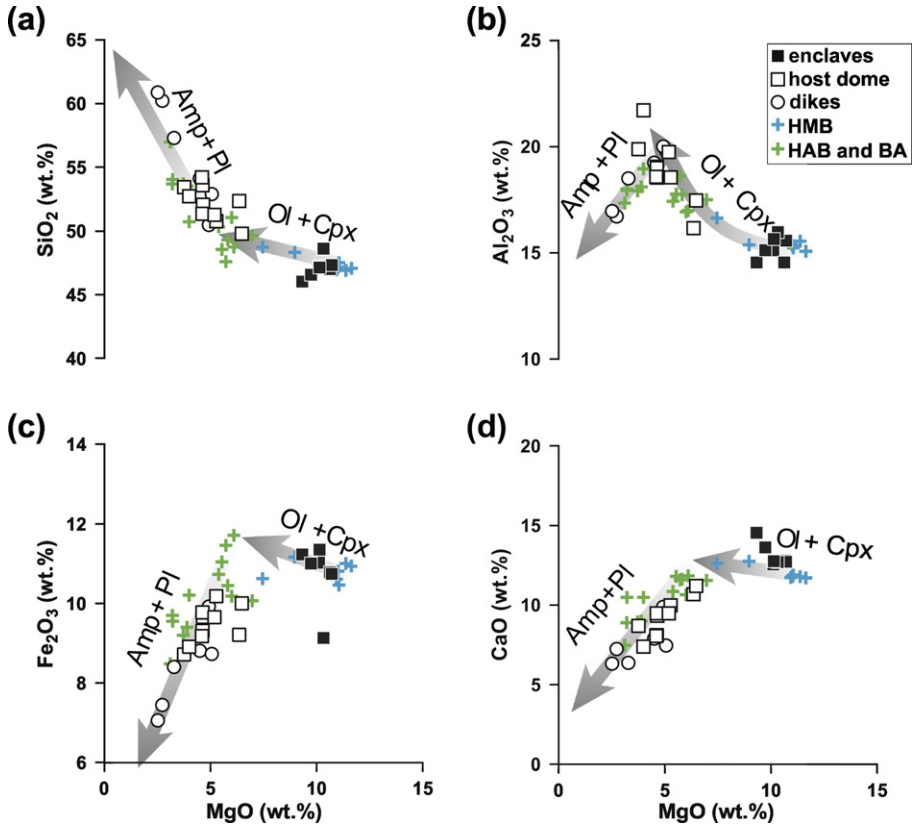

Fig. 6. Bulk-rock compositions of products from the CMVD are plotted in the MgO vs. SiO_2 (a), Al_2O_3 (b), Fe_2O_3 (c), and CaO (d) diagram (error bars within the symbols). Arrows indicate the prevalent fractionation of Fo-rich olivine (Ol) + Type 1 clinopyroxene (Cpx) and amphibole (Amp) + An-rich plagioclase (Pl). Data from this study are also compared with the Montresta compositions reported by Morra et al. (1997), i.e., high-Mg basalts (HMB), more differentiated high-Al basalts (HAB), and basaltic andesites (BA).

succession at CMVD (cf. Morra et al., 1997), especially for their extremely low concentrations of LREE (Fig. 7a) and incompatible trace element (mostly HFSE; Fig. 7b). In contrast, enclaves are plainly more similar to the more evolved HAB and BA products.

In this view, crystal-rich enclaves do not indeed represent the parental magma composition but rather a derivative melt from a primitive precursory crystallising primitive olivines ($Fo_{84–87}$), Type 1 clinopyroxenes ($Mg\#_{83–91}$), and Cr-spinel. Through the Fe—Mg exchange between olivine/clinopyroxene and melt, the composition of such primitive progenitor has been recalculated assuming equilibrium exchange partition coefficients of ${}^{ol\text{-}melt}Kd_{Fe–Mg} = 0.30 \pm 0.03$ (Roeder and Emslie, 1970) and ${}^{cpx\text{-}melt}Kd_{Fe–Mg} = 0.27 \pm 0.03$ (Putirka et al., 2003). It is found that $Fo_{84–87}$ olivines and $Mg\#_{83–91}$ Type 1 clinopyroxenes from enclaves are, on average, in equilibrium with magmas ($Mg\#_{64–65}$) resembling the compositions ($Mg\#_{58–68}$) of HMB products erupted at Montresta. Therefore, the most primitive HMB rock is recognised as the parental magma at CMVD.

To confirm this hypothesis, mass balance calculations have been performed to quantify the degree of crystallisation driving the HMB magma towards BA and andesitic compositions. A two-step calculation approach has been adopted by subtracting 1) the enclave coarse-grained paragenesis (i.e., Fo_{86} olivine + $Mg\#_{87}$ Type 1 clinopyroxene + $Mg\#_{73}$ amphibole + An_{91} plagioclase + Usp_5 titanomagnetite) to the composition of HMB, and 2) the crystal clot paragenesis (i.e., $Mg\#_{67}$ amphibole + An_{90} plagioclase + Usp_{30} titanomagnetite) to the residual melt derived by step 1 (see details in Table 8B). The MgO vs. TiO_2 diagram (Fig. 8) shows that enclave compositions cannot be reproduced by simple subtraction of minerals to the parental HMB magma, i.e., the sum of squared residuals (SSR) is higher than 1, denoting weak statistics for step 1. In contrast, the host dome composition is fairly reproduced (SSR = 0.44) by the crystallisation of olivine (~11%) + Type 1 clinopyroxene (~16%) + amphibole (~12%) + plagioclase (~11%) + titanomagnetite (~3%). In step 2 (Fig. 8), the dike composition is also adequately reconstructed (SSR = 0.13) by subtraction of amphibole (~23%) + plagioclase (~16%) + titanomagnetite (~3%). Results from mass balance calculations indicate that the segregation of primitive Type 1 clinopyroxene plays a major role at the early stage of HMB differentiation to form BA. On the contrary, the late crystallisation of $Mg\#_{67}$ amphibole + An_{90} plagioclase (i.e., the crystal clot paragenesis) drives the magmatic evolution from BA to andesites, accounting for the prevalent segregation of amphibole over plagioclase.

The negative correlation between Al_{tot} and Mg# observed for Type 1 clinopyroxene (Fig. 2d) is consistent with a progressive Al_2O_3 enrichment in the primitive magma crystallising clinopyroxene. Accordingly, this tendency is reflected by the increase of Al_2O_3 with decreasing MgO from HMB to BA (Fig. 6b), pointing to the early crystallisation of mafic minerals (i.e., clinopyroxene and olivine) with typically low Al_2O_3 concentrations rather than feldspar. The crystallisation of olivine also influences the early differentiation of HMB, in agreement with the almost constant CaO content of magma when MgO varies between 7 and 12 wt% (Fig. 6d). Moreover, the textural association of Fo-rich olivine + Cr-spinel suggests that this latter mineral cosaturated the melt at the onset of olivine crystallisation, before the formation of Type 1 clinopyroxene (cf. Morra et al., 1997).

Textural evidence point out that the crystallisation of primitive (~$Mg\#_{75}$) amphibole occurs at higher temperature than plagioclase. On one hand, centimetre-sized, $Mg\#_{68–71}$ amphiboles from enclaves, showing the lowest Al_{tot} concentrations (2.2–2.6 apfu; Fig. 3d), are observed to frequently entrap small $An_{72–93}$ plagioclase crystals. On the second hand, the more primitive ($Mg\#_{71–76}$) and Al-rich (Al_{tot} = 2.6–2.8 apfu) amphiboles do not exhibit mineral inclusions. Analogously, plagioclase inclusions are almost lacking in the more primitive ($Mg\#_{70–73}$) and Al-rich (Al_{tot} = 2.5–2.6 apfu) amphibole from the coarse-grained crystal clots (Fig. 3d, e), whereas feldspar abundance

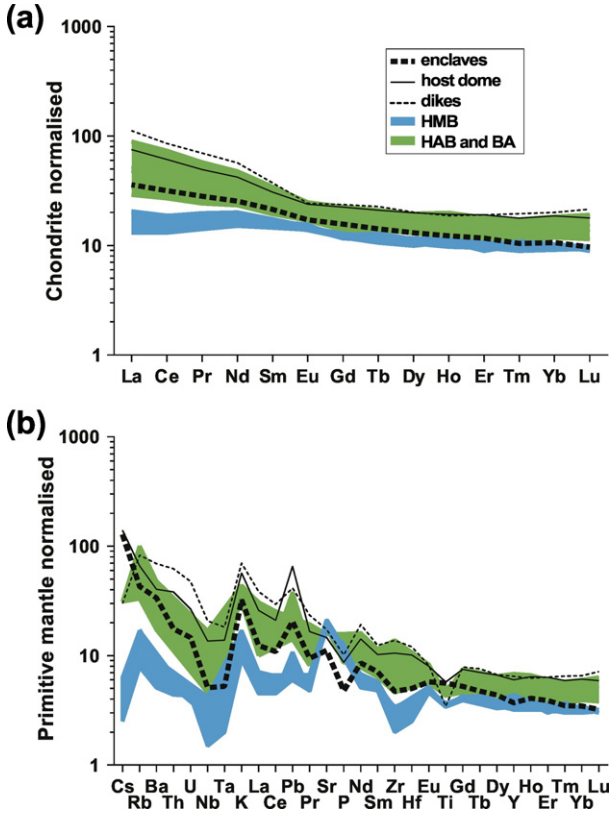

Fig. 7. Chondrite-normalised patterns of Rare Earth Elements (REE) (a) and primitive mantle-normalised trace element patterns (b). Data from this study (error bars within the symbols) are also compared with the Montresta compositions reported by Morra et al. (1997), i.e., high-Mg basalts (HMB), more differentiated high-Al basalts (HAB), and basaltic andesites (BA).

increases significantly in the medium-grained samples where more evolved amphiboles ($Mg\#_{60–69}$ and Al_{tot} = 2.2–2.5 apfu) crystallise (Fig. 3f). This leads to the conclusion that the crystallisation sequence of HMB products is Fo-rich olivine (± Cr-spinel) + primitive Type 1 clinopyroxene + high-Mg# amphibole + An-rich plagioclase. Olivine

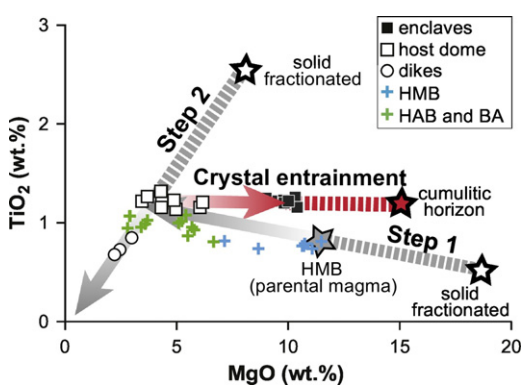

Fig. 8. MgO vs. TiO_2 diagram from modelling data in Table 8B (error bars within the symbols). A two-step calculation has been performed by subtracting 1) the enclave coarse-grained paragenesis (i.e., Fo_{86} olivine + $Mg\#_{87}$ Type 1 clinopyroxene + $Mg\#_{73}$ amphibole + An_{91} plagioclase + Usp_5 titanomagnetite) to the composition of HMB, and 2) the crystal clot paragenesis (i.e., $Mg\#_{67}$ amphibole + An_{90} plagioclase + Usp_{30} titanomagnetite) to the residual melt derived by step 1. The host dome composition is fairly reproduced (SSR = 0.44) by the crystallisation of olivine (~11%) + Type 1 clinopyroxene (~16%) + amphibole (~12%) + plagioclase (~11%) + titanomagnetite (~3%). For the case of step 2, the dike composition is also adequately reconstructed (SSR = 0.13) by subtraction of amphibole (~23%) + plagioclase (~16%) + titanomagnetite (~3%). The enclave compositions are well reproduced (SSR = 0.02–0.04) by the addition of Fo_{86} olivine (3–4%), $Mg\#_{87}$ Type 1 clinopyroxene (20–21%), $Mg\#_{73}$ amphibole (20–21%), An_{91} plagioclase (5–6%) and Usp_5 titanomagnetite (2–3%) to the basaltic andesitic magma.

and Type 1 clinopyroxene control the early differentiation of magma, despite being not the only mineral phases to be crystallised during the HMB to BA evolution (step 1). Conversely, amphibole and plagioclase progressively dominate the latest stage of magma differentiation towards andesitic compositions (step 2). Assuming equilibrium crystallisation when ${}^{amp\text{-}melt}Kd_{Fe–Mg} = 0.34 \pm 0.06$ (cf. Li et al., 2017), the most primitive $Mg\#_{76}$ amphiboles from enclaves are effectively in equilibrium with the HAB magma (i.e., sample CM43 with $Mg\#_{52}$). On the contrary, the late formation of An-rich plagioclase is attested by the negative trajectory in the Al_2O_3 vs. MgO diagram (Fig. 6b); this is dictated by abundant feldspar fractionation in correspondence of the more differentiated ($<Mg\#_{50}$) BA and andesitic terms.

6.2. Trace element modelling

Due to the scarce sensitivity of major elements to open-system contamination phenomena, bulk-rock trace element modelling can more adequately clarify the geochemical evolution of CMVD products during interaction between magma and crustal materials. Indeed, geochemical data for Montresta products indicate that crustal contamination plays a focal role in the evolution of magma (Franciosi et al., 2003; Morra et al., 1997). Coherently, Sr isotope ratios have been commonly observed to increase from basalts to andesites (Brotzu et al., 1997a; Dupuy et al., 1974; Lonis et al., 1997; Lustrino et al., 2013; Morra et al., 1997), suggesting that contamination phenomena take place within the middle-lower crust, at depths of 20–30 km (i.e., 500–700 MPa; Coulon et al., 1978 and Morra et al., 1994). Sr isotope ratios reported by Morra et al. (1997) increase from ~0.704 to ~0.706, along with variations in SiO_2 and incompatible trace elements from HMB to andesitic rocks. FC (fractional crystallisation) and AFC (assimilation and fractional crystallisation) modelling conducted by these authors denote that HMB magmas assimilated up to 13% of granitoid materials from the sialic lower crust (${}^{87}Sr/{}^{86}Sr$ = ~0.715).

In this view, we have modelled the geochemical behaviour of transition elements (i.e., Cr and Ti), HFSE (i.e., Zr), and REE (i.e., La, Ce, Nd, Sm, Eu, Gd, Dy, Er, Yb and Lu) during FC and AFC processes at CMVD. According to the Rayleigh fractionation law, FC is expressed as:

$$C_l = C_0 \cdot F^{D-1}$$

where C_0 and C_l are, respectively, the concentrations of the trace element in parental liquid and melt remaining during fractional crystallisation. F is the melt fraction and D is the bulk partition coefficient of the element for the n-fractionating mineral phases, calculated as:

$$D = \sum_i^n x_i \cdot K_{D_i}$$

with x_i as the weight fraction of mineral phase i and K_{Di} as the partition coefficient of the element in mineral phase i. In turn, AFC is formulated after DePaolo (1981):

$$C_l = C_0\left[F^{-z} + \left(\frac{r}{r-1}\right) \cdot \frac{C_a}{z \cdot C_0} \cdot \left(1 - F^{-1}\right)\right]$$

with C_0, C_l, D, and F as above. C_a is the concentration of the element of interest in the contaminant (wall rock), whereas r is the mass ratio of assimilated to crystallised material. The value of z can be derived as:

$$z = \frac{r + D - 1}{r - 1}$$

Following the strategy designed for mass balance calculations, a two-step modelling approach is adopted. The most primitive basalt from HMB and the less differentiated basaltic andesite at CMVD are used as starting compositions. Two distinct vectors are calculated for step 1 and step 2, accounting for either prevalent fractionation of

Fo-rich olivine + primitive Type 1 clinopyroxene (i.e., FC1 and AFC1), or $Mg\#_{67}$ amphibole + An_{90} plagioclase (i.e., FC2 and AFC2). The assimilant composition comes from Tommasini et al. (1995) and corresponds to the Hercynian granite from Sardinian-Corsan Batholith, as inferred by Brotzu et al. (1997a) and Conte (1997). Values for F and x_i are those recovered by mass balance calculations (Table 8B). Input and output data concerning FC and AFC modelling are listed in Table 9B, together with the values of partition coefficients specifically derived for calc-alkaline magmas (i.e., Bacon and Druitt, 1988; Dostal et al., 1983; Duke, 1976; Dunn and Sen, 1994; Forsythe et al., 1994; Frey, 1969; Fujimaki et al., 1984; Green et al., 1993; Irving and Frey, 1984; Jones and Drake, 1986; Klöck and Plame, 1988; Luhr and Carmichael, 1980; McKay and Weill, 1976; McKay et al., 1994; Oberti et al., 2000; Okamoto, 1979; Reid, 1983; Skulski et al., 1994; Villemant et al., 1981).

The Y vs. Cr diagram (Fig. 9) shows that, after ~53% of mineral segregation, FC and AFC vectors from step 1 and step 2 virtually overlap. The residual melt composition changes slightly under the effect of fractional crystallisation (Y ≈ 32 ppm and Cr ≈ 0.4 ppm) and country rock assimilation (Y ≈ 33 ppm and Cr ≈ 0.2 ppm). The evolutionary trajectories evidence as HMB products are mostly dominated by fractionation of mafic minerals (i.e., FC1 and AFC1), whereas the differentiation of basaltic andesites to andesites proceeds by $Mg\#_{67}$ amphibole and An_{90} plagioclase saturation (i.e., FC2 and AFC2; Fig. 9). In terms of LREE vs. HFSE ratios (Fig. 10a), the FC1 vector cannot reproduce in full the transition from HMB magmas to basaltic andesites. This geochemical evolution is captured only by the AFC1 vector when the ratio of the assimilation rate to the crystallisation rate (i.e., $r = 0.16$) is close to the degree of assimilation derived by Morra et al. (1997). On the other hand, both FC2 and AFC2 trajectories describe plausible differentiation paths for the basaltic andesitic magmas (Fig. 10a). The AFC2 vector denotes lower degrees of contamination (i.e., $r = 0.1$) for the more differentiated melts, perhaps responding to the colder thermal regime of the system (cf. Bohrson and Spera, 2001). The same conclusion applies to the behaviour of REE (Fig. 10b). The crustal contribution is more effective during step 1, producing remarkable LREE enrichments in the basaltic andesitic melt.

The role played by crustal assimilation during the geochemical evolution of magma is also documented by Sr isotope data for Montresta products (Fig. 11a). Modelling results (Table 10B) based on the formalism of DePaolo (1981) indicate that the parental HMB magma ($^{87}Sr/^{86}Sr$ = 0.7039) differentiated towards the andesitic rocks ($^{87}Sr/^{86}Sr$ = 0.7062–0.7068) by assimilation of the Hercynian crust ($^{87}Sr/^{86}Sr$ = 0.732). To estimate the maximum degree of assimilation, the energy-constrained

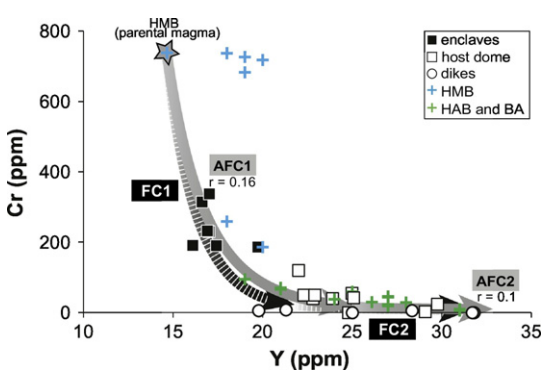

Fig. 9. Y vs. Cr diagram from fractional crystallisation (FC) and assimilation and fractional crystallisation (AFC) calculations (error bars within the symbols). Two distinct vectors are calculated accounting for the prevalent fractionation of Fo-rich olivine + Type 1 clinopyroxene (i.e., FC1 and AFC1) and $Mg\#_{67}$ amphibole + An_{90} plagioclase (i.e., FC2 and AFC2). The assimilant composition comes from Tommasini et al. (1995) and corresponds to the Hercynian granite from Sardinian-Corsan Batholith. Input and output data concerning FC and AFC modelling are listed in Table 9B, together with the values of partition coefficients derived for calc-alkaline magmas.

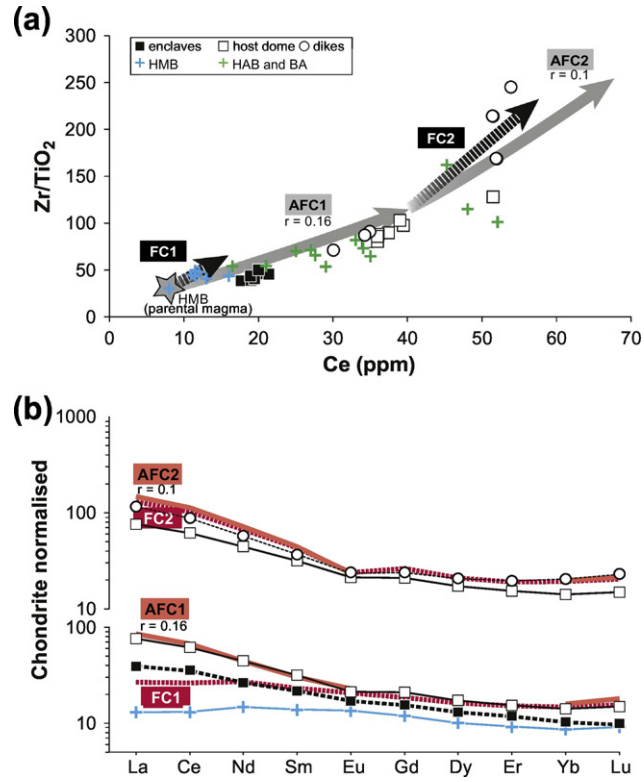

Fig. 10. Ce vs. Zr/TiO_2 ratio from fractional crystallisation (FC) and assimilation and fractional crystallisation (AFC) calculations (a). Two distinct vectors account for the prevalent fractionation of Fo-rich olivine + Type 1 clinopyroxene (i.e., FC1 and AFC1) and $Mg\#_{67}$ amphibole + An_{90} plagioclase (i.e., FC2 and AFC2). See Table 9B for further details. The FC1 vector cannot reproduce in full the transition from HMB magmas to basaltic andesites. This geochemical evolution is captured only by the AFC1 vector when the ratio of the assimilation rate to the crystallisation rate is $r = 0.16$. Both FC2 and AFC2 trajectories describe plausible differentiation paths for the basaltic andesitic magmas. The AFC2 vector denotes lower degrees of contamination for the more differentiated products with $r = 0.1$. REE patterns from the same calculations described above confirm that crustal contribution is more effective during step 1, producing strong LREE enrichments in the basaltic andesitic melt (b). Error bars are within the symbols.

assimilation–fractional crystallisation (EC-AFC) formulation of Spera and Bohrson (2001) has been used (Fig. 11b). This model builds on previous treatments of open-system processes (e.g., DePaolo, 1981) but it also considers the mass, chemical, and thermal properties of a magma body, as well as the energy conservation and country rock partial melting. According to Bohrson and Spera (2001), the input parameters for the granitic country rock are solidus (675 °C) and liquidus (950 °C) of the assimilant with isobaric specific heat capacity of 1388 J kg^{-1} K^{-1}, whereas those of magma are the liquidus temperature (1250 °C) and isobaric specific heat capacity of 1555 J kg^{-1} K^{-1}. The mass of fractionated material is much higher than that of crustal rock assimilated, causing that the highest $^{87}Sr/^{86}Sr$ ratio measured for HMB products is related to a maximum crustal assimilation of 10% and fractional crystallisation of 55% (Fig. 11b). Both these derived values conform to (i) the high radiogenic nature of the Hercynian basement of Sardinia island (Di Vincenzo et al., 1996), (ii) the trace element patterns of CMVD rocks (Fig. 10), and (iii) the review study of Lustrino et al. (2013) denoting as the degree of assimilation cannot exceeds the value of ~20% during interaction between primitive Sardinian basalts and Hercynian basement.

6.3. Origin of enclaves

Textural (Figs. 2 and 3), mineralogical (Fig. 4), and geochemical (Figs. 7 and 8) data point out that the formation of enclaves is controlled by evolutionary mechanisms rather different from those driving the petrogenesis of basaltic andesitic and andesitic rocks. Importantly, the

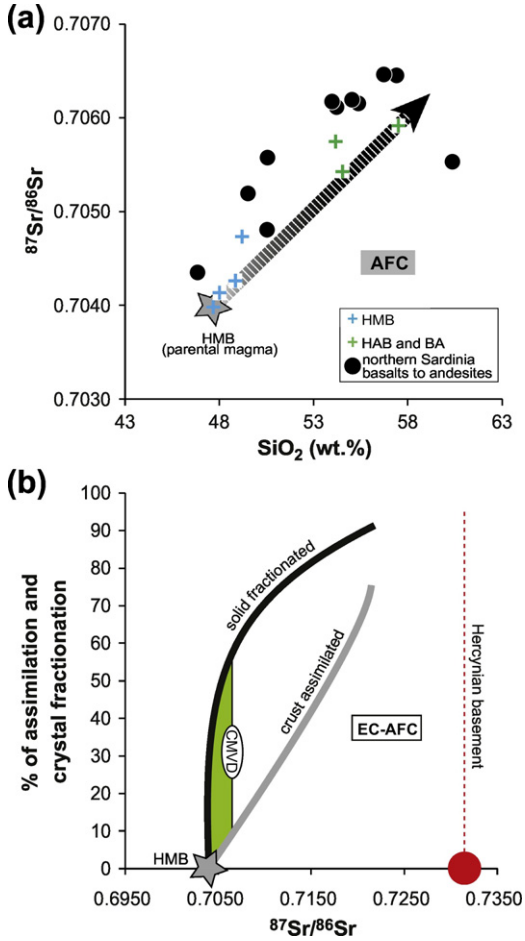

Fig. 11. SiO_2 vs. $^{87}Sr/^{86}Sr$ ratio (error bars within the symbols) of Montresta and northern Sardinia products (a). Modelling data (Table 10B) from DePaolo (1981) indicate that the parental HMB magma ($^{87}Sr/^{86}Sr = 0.7039$) differentiated towards the andesitic rocks ($^{87}Sr/^{86}Sr = 0.7062–0.7068$) by assimilation of the Hercynian crust ($^{87}Sr/^{86}Sr = 0.732$). The energy-constrained assimilation–fractional crystallisation (EC-AFC) formulation of Spera and Bohrson (2001) points out that the highest $^{87}Sr/^{86}Sr$ ratio measured for HMB products is related to a maximum crustal assimilation of 10% and fractional crystallisation of 55% (b).

overgrowth of Type 2 clinopyroxene rims on early-formed Type 1 cores (Fig. 2a) evidences open-system magma dynamics ascribable to entrainment of early-formed crystals in a compositionally distinct melt (Dungan and Davidson, 2004; Streck, 2008; Streck et al., 2007). Sharp transitions from Mg-rich (Type 1) to Mg-poor (Type 2) mineral portions (Figs. 2a) and resorption textures forming patchy zoning (Fig. 2b) are both the effect of pervasive dissolution phenomena followed by crystal re-equilibration (Streck, 2008). Reaction minerals in amphibole coronas (i.e., clinopyroxene + plagioclase + titanomagnetite/ilmenite ± low-Ca pyroxene; Fig. 3c) developed at the interface with a more differentiated magma that, in turn, underwent abundant groundmass crystallisation at the time of eruption. Additionally, HAB products and enclaves share a common trace element signature (Fig. 7) indicative of cogenetic origin. In this framework, it is argued that enclaves represent the crystal-rich portion of a volatile-rich, basaltic magma stored at depth and in equilibrium with Type 1 clinopyroxene and $Mg\#_{73–75}$ amphibole (cf. Stamper et al., 2014). Conversely, the sharp textural discontinuity between Type 1 and Type 2 clinopyroxenes denotes the injection of a compositionally distinct magma (Fig. 2a). Field and petrographic characters of the host dome evidence that the basaltic andesitic melt infiltrated, disaggregated and reacted within the cumulate horizon, feeding the overgrowth of Type 2 clinopyroxene rims onto Type 1 cores (Fig. 1c). The dome formation is indeed petrogenetically related to the emplacement of a more differentiated melt carrying crystal-rich enclaves. During magma ascent, rapid decompression and volatile loss may have caused the progress of amphibole reaction coronas (e.g., De De Angelis et al., 2015) and the crystallisation of a more sodic plagioclase in equilibrium with basaltic andesitic to andesitic melts (e.g. Frey and Lange, 2011). According to Ruprecht and Wörner (2007), the abrupt shifts in the anorthite component associated to almost constant iron concentrations are consistent with crystallisation under variable temperature and/or partial pressure of H_2O upon magma ascent in the volcanic conduit. In this context, the compositional trend observed for plagioclase from host dome (from An_{90} phenocryst cores to An_{45} microlites with ~0.6 wt% FeO) may effectively result from a higher efficacy of decompression-induced degassing (e.g., Blundy and Cashman, 2001) rather than heating during ascent-driven crystallisation and latent heat release (Blundy et al., 2006).

On this basis, the least square method has been used to model the composition of the enclaves by entrainment of Fo_{86} olivine + $Mg\#_{87}$ Type 1 clinopyroxene + $Mg\#_{73}$ amphibole + An_{91} plagioclase + Usp_5 titanomagnetite in the basaltic andesitic host dome. The mineral compositions adopted for the calculation correspond to those previously used to model magma fractional crystallisation (step 1; Table 8B). Modelling data confirm that the enclave compositions are well reproduced (SSR = 0.02–0.04) by addition of olivine (3–4%), Type 1 clinopyroxene (20–21%), amphibole (20–21%), plagioclase (5–6%) and titanomagnetite (2–3%) to the basaltic andesitic magma (Fig. 8). In terms of trace element contents, Sc (74–81 ppm) and V (457–474 ppm) measured for the enclaves are intriguingly higher than transition elements typically measured for Island Arc Basalts (i.e., IAB with Sc ≤ 55 ppm and V ≤ 450 ppm; cf. Doe, 1997). The high compatibility of scandium in clinopyroxene and amphibole is controlled by its ionic radius (74.5 pm in six-fold coordination) and electronegativity (1.36 from the Pauling's scale) that are both very similar to those (72 pm and 1.31, respectively) of magnesium (Iain and Chassé, 2016). The geochemical behaviour of vanadium resembles that of scandium, despite the fact that vanadium can be more favourably incorporated in Mg-rich amphiboles due to the crystal-chemical control effect on trace element partitioning (Meurer and Claeson, 2002). Consequently, partition coefficients of Sc and V for clinopyroxene ($K_{Sc} = 2.5$ and $K_V = 2.3$; Dale and Henderson, 1972 and Duke, 1976), amphibole ($K_{Sc} = 4$ and $K_V = 1.49$; Sisson, 1994), and titanomagnetite ($K_{Sc} = 3{,}3$ and $K_V = 6.8$; Luhr and Carmichael, 1980 and Nielsen, 1992) are much higher than those measured for olivine ($K_{Sc} = 0.3$ and $K_V = 0.08$; Luhr and Carmichael, 1980 and Duke, 1976) and plagioclase ($K_{Sc} = 0.02$ and $K_V = 0.02$; Luhr and Carmichael, 1980 and Dunn and Sen, 1994). Eluding

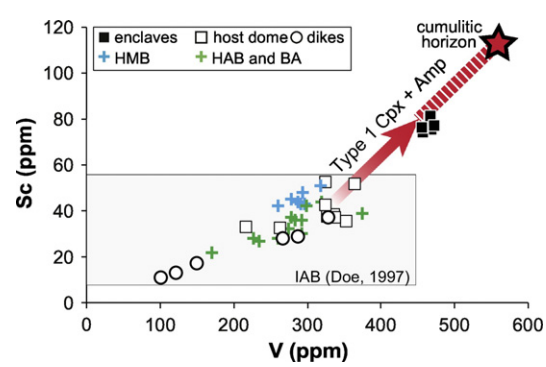

Fig. 12. V vs. Sc diagram showing as the trace element contents measured for the enclaves (error bars within the symbols) are intriguingly higher than transition elements typically measured for Island Arc Basalts (i.e., IAB; cf. Doe, 1997). The vector accounts for the entrainment of Type 1 clinopyroxene and amphibole within the basaltic andesitic host dome. The concentrations of V and Sc in Type 1 clinopyroxene and amphibole crystals come from equilibrium partitioning calculations performed on HMB (sample KBLF) and HAB (sample CM43) compositions (further details are given in Table 11B). Enclaves lie on a mixing trajectory resulting from entrainment of Type 1 clinopyroxene (51%) and amphibole (49%) in the basaltic andesitic magma (the mineral content corresponds to mass balance data normalised to 100).

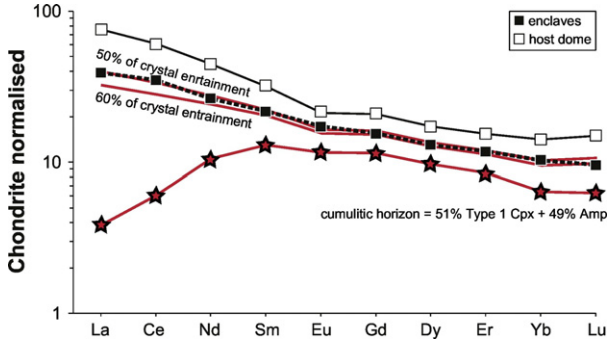

Fig. 13. Mixing calculations for REE attest that enclave compositions (error bars within the symbols) are associated with hybridisation phenomena due to entrainment of a solid fraction (50–60%) of Type 1 clinopyroxene and $Mg\#_{71-76}$ amphibole into the original basaltic andesitic magma. See Table 11B for further details.

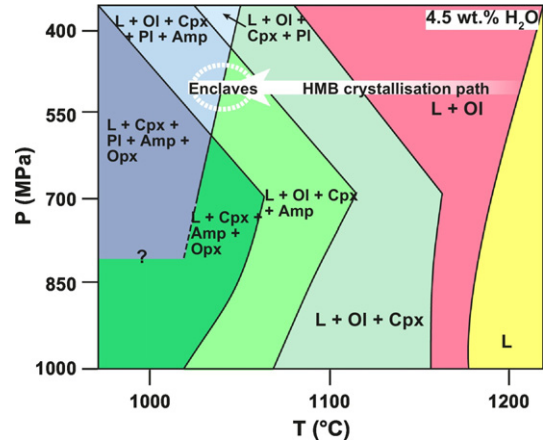

Fig. 14. Phase relations for a calc-alkaline high-Mg basalt equilibrated at $P = 400–1000$ MPa, $T = 1000–1200$ °C, $H_2O = 4.5$ wt%, and $fO_2 = NNO\text{-}NNO + 4$. (cf. Pichavant and Macdonald, 2007; Melekhova et al., 2015). Abbreviations indicate: Ol, olivine; Cpx, clinopyroxene; Opx, orthopyroxene; Amp, amphibole; Pl, plagioclase; L, liquid. Amphibole saturates the primitive basaltic liquid after the crystallisation of olivine, Cr-spinel, and clinopyroxene but before the onset of plagioclase at $P > 400$ MPa and $T > 1030$ °C.

the low solid fraction of titanomagnetite, the entrainment of Type 1 clinopyroxene and amphibole within the basaltic andesitic melt can be described by the following mixing expression:

$$C_m = X \cdot (C_s - C_{BA}) + C_{BA}$$

where C_s, C_{BA}, and C_m are the concentrations of the cumulate horizon, the basaltic andesite, and the final hybrid rock, whereas X is the degree of mixing. The concentrations of V and Sc in Type 1 clinopyroxene and amphibole crystals come from equilibrium partitioning calculations performed on HMB (sample KB24) and HAB (sample CM43) compositions (further details are given in Table 11B). The V vs. Sc diagram (Fig. 12) shows that enclaves lie on a mixing trajectory resulting from entrainment of Type 1 clinopyroxene (51%) and amphibole (49%) in the basaltic andesitic magma (note that the mineral content come from mass balance data normalised to 100). Through the same approach, modelling calculations for REE attest that enclave compositions result from hybridisation phenomena due to the entrainment of a pre-existing crystal cargo (50–60%) of Type 1 clinopyroxene + $Mg\#_{71-76}$ amphibole into the original basaltic andesitic magma (Fig. 13).

6.4. Magma crystallisation conditions

To retrieve the intensive variable of the magmatic system during evolution of HMB towards more differentiated basaltic andesites and andesites, phase equilibrium experiments of Grove et al. (2003), Pichavant and Macdonald (2007), and Melekhova et al. (2015) have been compared with the mineral assemblage of natural products from the CMVD. The compositions investigated by these authors consists of high-Mg basalts to andesites equilibrated at $P = 0.1–1500$ MPa, $T = 940–1350$ °C, $H_2O = 0–8$ wt% (from anhydrous to $P_{tot} = P_{H2O}$), and $fO_2 = QFM\text{-}NNO + 4$. Results show that, at $P > 400$ MPa and $H_2O > 2$ wt%, the stability field of both olivine and clinopyroxene expands at the expense of plagioclase (Fig. 14). Under such circumstances, the crystallisation of 30–40% of mafic minerals (cf. Pichavant and Macdonald, 2007) drives the residual melt towards compositions comparable to those observed for HAB and basaltic andesitic products from the CMVD (Figs. 5 and 6). At 400 MPa, 1000–1025 °C, 5–6 wt% H_2O, and NNO-0.8-NNO + 2.4 buffer, Pichavant and Macdonald (2007) found that amphibole equilibrates with high-Mg basaltic melts, after segregation of olivine + Cr-spinel + clinopyroxene + plagioclase. In contrast, the same authors document that, at 1000 MPa, 1044 °C, 9.4 wt% H_2O, and NNO + 2, amphibole occurs as the liquidus phase when the crystallisation of plagioclase is suppressed. As a rule, at $P > 400$ MPa, $T > 1030$ °C, $H_2O > 4.5$ wt%, and $fO_2 > NNO$, amphibole saturates the primitive basaltic liquid after the crystallisation of olivine, Cr-spinel, and clinopyroxene (Fig. 14) but, importantly, its appearance precedes the onset of plagioclase crystallisation (Grove et al., 2003; Melekhova et al., 2015; Pichavant and Macdonald, 2007). The chemistry of experimental amphiboles ($Mg\#_{72-79}$) is also very similar to that ($Mg\#_{71-76}$) of natural minerals from enclaves, providing further constraints on the formation of amphibole at high pressures, temperatures and melt-water contents (cf. Grove et al., 2003; Melekhova et al., 2015).

In this framework, barometric, thermometric, hygrometric, and oxygen barometric equations have been used to model the P-T-H_2O-fO_2 path of the system during the differentiation of HMB magmas towards more evolved basaltic andesitic and andesitic terms. The redox state of enclaves, crystal clots, host dome, and dikes has been measured through the equations of Ariskin and Nikolaev (1996), France et al. (2010), and Ridolfi et al. (2010) based on spinel-melt (error of ±0.3 log unit), clinopyroxene-plagioclase (error of ±0.5 log unit), and amphibole-melt equilibria (error of ±0.4 log unit), respectively. The input pressures and temperatures for these models have been obtained with the independent barometric and thermometric equations described below. Results from calculations are plotted in Fig. 15a showing that, within the calibration error of each model, the oxygen fugacity of the system is constrained between NNO and NNO + 2, with the majority of the estimates pointing to NNO + 1. This value is consistent with previous data obtained using ilmenite-magnetite pairs from the groundmass of HMB products at Montresta (Morra et al., 1997), as well as with the more oxidised conditions commonly encountered for the subduction-related magmatism (cf. Scarlato et al., 2017).

The amount of H_2O in equilibrium with plagioclase has been determined through the Ca—Na exchange experimentally-derived by Sisson and Grove (1993) for calc-alkaline systems. Despite the anorthite content of plagioclase is positively correlated with H_2O and temperature, the value of ${}^{pl\text{-}melt}Kd_{Ca-Na}$ is a proxy for the amount of H_2O dissolved in the melt (i.e., P-T independent hygrometer), provided that the effects of temperature and pressure are negligible for the equilibrium Ca—Na exchange (cf. Ushioda et al., 2014). ${}^{pl\text{-}melt}Kd_{Ca-Na}$ values (3.4–5.5) measured in this study evidence that An-rich plagioclases from enclaves and host dome equilibrated with a basaltic andesitic melt characterised by relatively high H_2O contents ranging from 4 to 6 wt% (Fig. 15b). This is also confirmed by the incorporation of octahedral aluminium in amphiboles from enclaves and crystal clots, translating to H_2O contents of 5.6–7.9 wt% (error of ±0.41 wt% H_2O), as predicted by the amphibole-based hygrometer of Ridolfi et al. (2010). In contrast, the more sodic plagioclase rims formed at the final stage of crystallisation (i.e., ${}^{pl\text{-}melt}Kd_{Ca-Na} = 1.7–3.4$), recording the lower H_2O concentrations (2–4 wt%) ultimately dissolved in host dome and dike andesitic magmas (Fig. 15b).

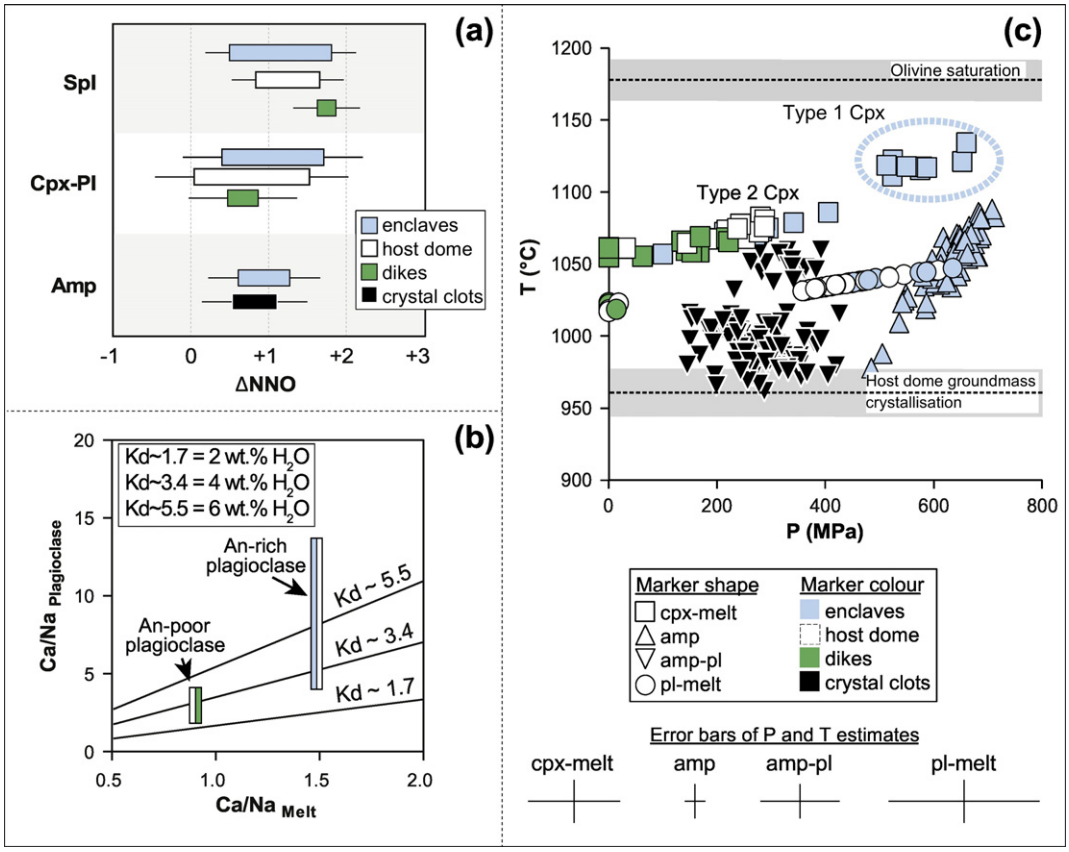

Fig. 15. Modelling data for the *P-T*-H_2O-fO_2 path of the system. The redox state of enclaves, host dome, dikes, and crystal clots (a) has been measured through the equations of Ariskin and Nikolaev (1996), France et al. (2010), and Ridolfi et al. (2010) based on spinel-melt (error of ±0.3 log unit), clinopyroxene-plagioclase (error of ±0.5 log unit), and amphibole-melt equilibria (error of ±0.4 log unit), respectively. The amount of H_2O in equilibrium with plagioclase has been determined through the Ca—Na exchange experimentally-derived by Sisson and Grove (1993) (b). Straight lines represent Ca—Na exchange partition coefficients derived by anhydrous ($^{pl\text{-}melt}Kd_{Ca-Na} = 1.1$) to H_2O-saturated ($^{pl\text{-}melt}Kd_{Ca-Na} = 5.5$) experiments. Bars represent the range of $^{pl\text{-}melt}Kd_{Ca-Na}$ measured for natural plagioclase from enclaves (light blue), host dome (white), and dikes (green). The saturation temperature of Fo_{84-87} olivines from enclaves (c) has been estimated with the thermometer (error of ±29 °C) of Putirka et al. (2007). The crystallisation pressure and temperature of clinopyroxene have been calculated integrating the barometer (error of ±140 MPa) of Neave and Putirka (2017) with the P-independent thermometer (error of ±27 °C) of Putirka et al. (1996). The crystallisation conditions of plagioclase have been constrained with the model (errors of ±240 MPa and ±26 °C) of Putirka (2005). Conversely, the formulations of Ridolfi et al. (2010) and Ridolfi and Renzulli (2012) have been adopted to retrieve, respectively, the saturation temperature (error of ±22 °C) and pressure (error of ±37 MPa) of amphibole. For the specific case of crystal clots, the barometer (error of ±150 MPa) of Molina et al. (2015) has been employed.

The crystallisation temperature of Fo_{84-87} olivines from enclaves has been estimated with the thermometer of Putirka et al. (2007) based on the partitioning of magnesium between forsterite and melt (error of ±29 °C). This model returns mineral saturation at 1176–1178 °C (Fig. 15c), in agreement with the stability field of olivine (1100–1220 °C) obtained in laboratory by Pichavant and Macdonald (2007) and Melekhova et al. (2015) at 400–700 MPa and 4.5 wt% H_2O (Fig. 14). The crystallisation pressure of clinopyroxene has been calculated with the recent *T*-dependent barometer (error of ±140 MPa) of Neave and Putirka (2017), referring to the pressure-sensitive incorporation of jadeite. This model has been integrated with the *P*-independent thermometer (error of ±27 °C) of Putirka et al. (1996) that, in turn, depends on the diopside-hedenbergite exchange.

The compositions of clinopyroxenes have been tested for equilibrium using the equation of Mollo et al. (2013) based on the difference (Δ) between diopside + hedenbergite (DiHd) components predicted for clinopyroxene via regression analysis of clinopyroxene-melt pairs in equilibrium conditions, and those measured in the analysed crystals. For the specific case of rocks with calc-alkaline affinity, phase equilibrium experiments indicate that near-equilibrium crystallisation conditions are achieved when the value of ΔDiHd is lower than 0.1 (Mollo et al., 2012). Type 1 clinopyroxenes ($Mg\#_{83-91}$) from enclaves yield pressures of 514–661 MPa and temperatures of 1111–1136 °C (Fig. 15c), in agreement with data from Pichavant and Macdonald (2007) and Melekhova et al. (2015) (Fig. 14). Type 2 clinopyroxenes ($Mg\#_{72-79}$) denote intermediate crystallisation conditions (i.e., 100–410 MPa and 1057–1086 °C) corresponding to the ascent of magma towards the surface. Conversely, the final closure temperature (1050–1085 °C) of the system is recorded by the more evolved clinopyroxenes ($Mg\#_{65-77}$) from host dome and dikes that, virtually, formed at the time of magma emplacement (0.1–280 MPa).

The crystallisation conditions of plagioclase have been constrained with the H_2O-dependent model of Putirka (2005) with errors of ±240 MPa and ±26 °C for pressure and temperature, respectively. The amount of H_2O in equilibrium with plagioclase has been modulated according to values recovered by the Ca—Na exchange reaction (Fig. 15b). However, we have established that a H_2O change of ±2 wt% produces temperature and pressures variations of only ±12 °C and ±15 MPa, which are well below the errors of estimates of the model.

The empirical formulations of Ridolfi et al. (2010) and Ridolfi and Renzulli (2012) have been adopted to retrieve, respectively, the saturation temperature (error of ±22 °C) and pressure (error of ±37 MPa) of amphibole. For the specific case of crystal clots, consistently with the petrography of these rocks, the barometer (error of ±150 MPa) of Molina et al. (2015) based on Al—Si partitioning between amphibole and plagioclase has been employed. Coherently with the textural characteristics of enclaves (Figs. 1d, 3a and b), these calculations suggest the early crystallisation of $Mg\#_{71-76}$ amphibole (978–1088 °C) respect to An-rich plagioclase (1031–1048 °C), at pressures of 355–713 MPa (Fig. 15c). On the other hand, the more evolved amphibole ($Mg\#_{60-69}$)

from crystal clots (Fig. 3e and f) is in cosaturation with An_{90} plagioclase at lower temperatures and pressures (i.e., 962–1060 °C and 145–427 MPa; Fig. 15c). Nonetheless, the more sodic plagioclase crystals from host dome and dikes equilibrated at the last stage of eruption (Fig. 15c) in a more degassed magma ascending along the uppermost part of the volcanic conduit (i.e., 0.1–16 MPa and 1017–1027 °C). Similarly, the two-pyroxene model of Putirka (2008) suggests near-equilibrium crystallisation (i.e., ${}^{cpx\text{-}opx}Kd_{Fe-Mg} = 1.09 \pm 0.14$) for low-Ca pyroxenes and augites in the host dome groundmass, providing information on the final quenching temperature during lava flowage onto the surface (i.e., 961–970 °C with error of ±38 °C).

Enclaves are interpreted as the cumulate assemblage of a high-temperature, water-rich magma stored at depth with composition close to that of HMB products (Fig. 15c). The segregation of mafic crystals at relatively high crustal pressures has been documented for basaltic rocks from Montresta (>500 MPa; Morra et al., 1997), as well as for the more differentiated products outcropping at both the northern and southern parts of Sardinia (500–700 MPa; Coulon et al., 1978 and Morra et al., 1994). In this scenario, the enclaves formed prevalently by Fo-rich olivine + primitive Type 1 clinopyroxene + high-Mg# amphibole accumulation and, minor An-rich plagioclase + titanomagnetite fractionation. Similarly, crystal clots represent the solid fractionated by a colder, hydrous basaltic andesite in a shallower region of the CMVD plumbing system, where the simultaneous precipitation of more evolved amphibole and An-rich plagioclase was favoured. These two gabbroid assemblages may therefore be ascribed to different portions of the polybaric crystal mush formed during the multi-stage HMB to basaltic andesitic to andesitic differentiation (e.g. Cashman et al., 2017; Chadwick et al., 2013; Deering et al., 2011; Dufek and Bachmann, 2010). The stable paragenesis of infiltrating basaltic andesite consists of Type 2 clinopyroxene + An_{88-93} plagioclase + titanomagnetite, followed by late groundmass crystallisation at the time of eruption. Type 2 clinopyroxenes are euhedral and compositionally homogeneous (Fig. 2c), in sharp contrast with the pervasive dissolution phenomena forming the spongy cellular texture of Type 1 crystals (Fig. 2b). Moreover, augitic Type 2 clinopyroxenes ($Mg\#_{72-79}$ and $Al_{tot} = 0.211–0.230$ apfu) are comparatively more evolved than diopsidic Type 1 clinopyroxenes (Fig. 2d), accounting for magma dynamics controlled by progressive melt evolution and crystal entrainment. Therefore, enclaves and crystal clots were entrapped by cogenetic magmas formed from the same HMB progenitor, as attested by modelling data (Figs. 8, 9, and 10) and the strong correlation coefficients ($R^2 = 0.86–0.96$) measured for the incompatible trace element ratios (e.g., La/Ce = 0.41–0.53 and Zr/Hf = 30–46).

7. Conclusions

This study focused on better understanding the textural and compositional characteristics of crystal-rich enclaves sampled from an andesitic dome outcropping at the Capo Marargiu Volcanic District (Sardinia island, Italy). Based on petrological and geochemical evidence, the following conclusions can be drawn:

1) enclaves formed during crystallisation of high-Mg basalts with trace element patterns resembling those of more differentiated basaltic andesitic to andesitic products found in the same stratigraphic succession;
2) diopsidic clinopyroxene and high-Mg# amphibole from enclaves show strong disequilibrium textures caused by entrainment in magmas that, subsequently, underwent decompression and volatile loss;
3) the mineral chemistry of enclaves reflects crystallisation in a high-temperature, high-pressure environment under water-rich conditions. In contrast, low-Mg# amphibole and An-rich plagioclase cosaturation recorded by crystal clots in andesites indicate crystallisation under hydrous conditions in a colder and shallower region of the plumbing system. In the end, phenocryst compositions from the more differentiated products constrain the final *P-T*—H_2O path of magma during ascent towards the surface.
4) enclaves and crystal clots represent different portions of a polybaric mush column formed during the two-step HMB to basaltic andesitic to andesitic differentiation. In particular, enclaves are the "cryptic" solid fraction of a cumulate horizon segregated from the deep-seated crystallisation of parental magma driven by Fo_{87} olivine + $Mg\#_{90}$ clinopyroxene, whereas crystal clots belong to the cumulate removed during the shallow fractionation of $Mg\#_{65}$ amphibole + An_{90} plagioclase from the basaltic andesite extracted at depth;
5) the geochemical signature of basalts, basaltic andesites, and andesites at Capo Marargiu Volcanic District has been also influenced by variable degrees of crustal assimilation involving the Hercynian granitic basement, with the highest contamination during the early evolutionary stage of parental magma in proximity of the Moho.

Supplementary data to this article can be found online at https://doi.org/10.1016/j.jvolgeores.2017.09.007.

Acknowledgements

We gratefully acknowledge Joan Andújar and an anonymous reviewer for their useful and constructive criticisms. The authors thank also J. Marti for his valuable editorial guidance. V.T. is grateful to F. Forni, A. Parmigiani (tetris), and J. Leuthold for their suggestions during the preparation of the manuscript. M. Nazzari is acknowledged for assistance during electron microprobe analysis. The authors are grateful to V. Piras for the logistic support on the field. This work was supported by the Sapienza - Università di Roma doctoral scholarship.

Appendix A. Analytical methods

Major element analyses of minerals (Tables 2B–6B) were carried out with a Jeol-JXA8200 microprobe installed at the HPHT Laboratory of Experimental Volcanology and Geophysics of the Istituto Nazionale di Geofisica e Vulcanologia (INGV) in Rome, Italy. The accelerating voltage and beam current were 15 kV and 10 nA, respectively. The beam size was 5 μm with a counting time of 20 and 10 s on peaks and background, respectively. The following standards have been adopted for the various chemical elements: jadeite (Si and Na), corundum (Al), forsterite (Mg), andradite (Fe), rutile (Ti), orthoclase (K), barite (Ba), apatite (P), spessartine (Mn) and chromite (Cr). Sodium and potassium were analysed first to prevent alkali migration effects. The precision of the microprobe was measured through the analysis of well-characterised synthetic oxides and minerals. Data quality was ensured by analysing these test materials as unknowns according to Iezzi et al. (2014).

Images were collected at the INGV using the backscattered electron (BSE) mode of a field emission gun-scanning electron microscopy (FE-SEM) Jeol 6500F equipped with an energy-dispersive spectrometer (EDS) detector.

Bulk-rock major element analyses (Table 7B) were performed at Department of Earth Sciences, Sapienza University of Rome (Italy) by X-ray fluorescence (Philips PW1480/10). The organic material was removed by sample washing, i.e., soaking in a hot mixture of HCl and H_2O_2 and cleaning in acetone using ultrasound. Loss-on-ignition (LOI) was calculated by measuring the weight loss from 2 g of powdered sample after heating to 1050 °C for 2 h. Then, 1 g of the devolatilised sample powder was mixed with di lithium tetraborate, melted in Pt crucibles at 1300 °C, and poured to form homogenous glassy beads. Matrix effects for major elements were corrected according to Franzini et al. (1972).

Bulk-rock trace element analyses (Table 7B) were measured at Actlabs (Activation Laboratories Ltd.) by lithium metaborate/tetraborate fusion – ICP-MS (inductively coupled plasma mass spectrometry). The fused samples were diluted and analysed by a Perkin Elmer Sciex ELAN 9000 ICP/MS. Three blanks and five controls (three before sample group and two after) were analysed per group of samples.

References

Abd El-Rahman, Y., Helmy, H.M., Shibata, T., Yoshikawa, M., Arai, S., Tamura, A., 2012. Mineral chemistry of the Neoproterozoic Alaskan-type Akarem intrusion with special emphasis on amphibole: implications for the pluton origin and evolution of subduction-related magma. Lithos 155:410–425. https://doi.org/10.1016/j.lithos.2012.09.015.

Alonso-Perez, R., Müntener, O., Ulmer, P., 2009. Igneous garnet and amphibole fractionation in the roots of island arcs: experimental constraints on andesitic liquids. Contrib. Mineral. Petrol. 157:541–558. https://doi.org/10.1007/s00410-008-0351-8.

Ariskin, A.A., Nikolaev, G.S., 1996. An empirical model for the calculation of spinel-melt equilibria in mafic igneous systems at atmospheric pressure: 1. Chromian spinels. Contrib. Mineral. Petrol. 123:282–292. https://doi.org/10.1007/s004100050156.

Avanzinelli, R., Lustrino, M., Mattei, M., Melluso, L., Conticelli, S., 2009. Potassic and ultrapotassic magmatism in the circum-Tyrrhenian region: significance of carbonated pelitic vs. pelitic sediment recycling at destructive plate margins. Lithos 113: 213–227. https://doi.org/10.1016/j.lithos.2009.03.029.

Bachmann, O., Dungan, M.A., 2002. Temperature-induced Al-zoning in hornblendes of the Fish Canyon magma, Colorado. Am. Mineral. 87, 1062–1076.

Bachmann, O., Huber, C., 2016. Silicic magma reservoirs in the Earth's crust. Am. Mineral. 101, 2377–2404.

Bacon, C.R., Druitt, T.H., 1988. Compositional evolution of the zoned calcalkaline magma chamber of mount Mazama, crater Lake, Oregon. Contrib. Mineral. Petrol. 98: 224–256. https://doi.org/10.1007/BF00402114.

Best, M.G., 1975. Amphibole bearing cumulate inclusions, Grand Canyon, Arizona, and their bearing on silica-undersaturated hydrous magma in the upper mantle. J. Petrol. 16, 212–236.

Blundy, J., Cashman, 2001. Ascent-driven crystallization of dacite magmas at Mount St Helens, 1980–1986. Contrib. Mineral. Petrol. 140, 631–650.

Blundy, J., Cashman, K., Humphreys, M., 2006. Magma heating by decompression-driven crystallization beneath andesite volcanoes. Nature 443, 76–80.

Bohrson, W.A., Spera, F.J., 2001. Energy-constrained open-system magmatic processes II: application of energy-constrained assimilation-fractional crystallization (EC-AFC) model to magmatic systems. J. Petrol. 42:1019–1041. https://doi.org/10.1093/petrology/42.5.1019.

Brotzu, P., Callegari, E., Morra, V., Ruffini, R., 1997a. The orogenic basalt-andesite suites from the tertiary volcanic complex of Narcao, SW-Sardinia (Italy): petrology, geochemistry and Sr-isotope characteristics. Period. Mineral. 66, 101–150.

Brotzu, P., Lonis, R., Melluso, L., Morbidelli, L., Traversa, G., Franciosi, L., 1997b. Petrology and evolution of calcalkaline magmas from the Arcuentu volcanic complex (SW Sardinia, Italy). Period. Mineral. 66, 151–184.

Carminati, E., Lustrino, M., Doglioni, C., 2012. Geodynamic evolution of the central and western Mediterranean: tectonics vs. igneous petrology constraints. Tectonophysics 579:173–192. https://doi.org/10.1016/j.tecto.2012.01.026.

Cashman, K.V., Sparks, R.S.J., Blundy, J.D., 2017. Vertically extensive and unstable magmatic systems: a unified view of igneous processes. Science 355, eaag3055.

Cawthorn, R.G., O'Hara, M.J., 1976. Amphibole fractionation in calc-alkaline magma genesis. Am. J. Sci. 276:309–329. https://doi.org/10.2475/ajs.276.3.309.

Chadwick, J.P., Troll, V.R., Waight, T.E., Van Der Zwan, F.M., Schwarzkopf, L.M., 2013. Petrology and geochemistry of igneous inclusions in recent Merapi deposits: a window into the sub-volcanic plumbing system. Contrib. Mineral. Petrol. 165, 259–282.

Cherchi, A., Mancin, N., Montadert, L., Murru, M., Putzu, M.T., Schiavinotto, F., Verrubbi, V., 2008. The stratigraphic response to the Oligo-Miocene extension in the western Mediterranean from observations on the Sardinia graben system (Italy). Bull. Soc. Geol. Fr. 179, 267–287.

Conte, A., 1997. Petrology and geochemistry of tertiary calcalkaline magmatic rocks from the Sarroch district (Sardinia, Italy). Period. Mineral. 66, 63–100.

Coulon, C., Baque, L., 1973. Les andésites cénozoiques et les laves associées en Sardaigne Nord-Occidentale (Provinces du Logudoro et du Bosano) - Caractères minéralogiques et chimiques. Contrib. Mineral. Petrol. 42:125–139. https://doi.org/10.1007/BF00371502.

Coulon, C., Demant, A., Bellon, H., 1974. Premieres datations par la methode K/Ar de quelques laves cenozoiques et quaternaires de Sardaigne nord-occidentale. Tectonophysics 22:41–57. https://doi.org/10.1016/0040-1951(74)90034-1.

Coulon, C., Dostal, J., Dupuy, C., 1978. Petrology and geochemistry of the ignimbrites and associated lava domes from NW Sardinia. Contrib. Mineral. Petrol. 68, 89–98.

Dale, I.M., Henderson, P., 1972. The partition of transition elements in phenocryst-bearing basalts and the implications about melt structure. 24th International Geological Congress, pp. 105–111.

Davidson, J., Turner, S., Handley, H., Macpherson, C., Dosseto, A., 2007. Amphibole "sponge" in arc crust? Geology 35:787–790. https://doi.org/10.1130/G23637A.1.

De Angelis, S.H., Larsen, J., Coombs, M., 2013. Pre-eruptive magmatic conditions at Augustine volcano, Alaska, 2006: evidence from amphibole geochemistry and textures. J. Petrol. 54, 1939–1961.

De Angelis, S.H., Larsen, J., Coombs, M., Dunn, A., Hayden, L., 2015. Amphibole reaction rims as a record of pre-eruptive magmatic heating: an experimental approach. Earth Planet. Sci. Lett. 426:235–245. https://doi.org/10.1016/j.epsl.2015.06.051.

DeBari, S.M., Coleman, R.G., 1989. Examination of the deep levels of an island arc: evidence from the Tonsina ultramafic-mafic assemblage, Tonsina, Alaska. J. Geophys. Res. 94, 4373–4391.

Deering, C.D., Bachmann, O., Dufek, J., Gravley, D.M., 2011. Rift-related transition from andesite to rhyolite volcanism in the Taupo Volcanic Zone (New Zealand) controlled by crystal-melt dynamics in mush zones with variable mineral assemblages. J. Petrol. 52, 2243–2263.

DePaolo, D.J., 1981. Trace element and isotopic effects of combined wallrock assimilation and fractional crystallization. Earth Planet. Sci. Lett. 53:189–202. https://doi.org/10.1016/0012-821X(81)90153-9.

Deriu, M., 1964. Notizie sulla costituzione geologica del Bosano, della Planargia e del Montiferro settentrionale e occidentale. e. Monografia Reg. Bosano, Ass. Comm. Bosa e Cuglieri, pp. 1–50.

Dessimoz, M., Muntener, O., Ulmer, P., 2012. A case for hornblende dominated fractionation of arc magmas: the Chelan Complex, Washington Cascades. Contrib. Mineral. Petrol. 163, 567–589.

Dieni, I., Massari, F., Médus, J., 2008. Age, depositional environment and stratigraphic value of the Cuccuru 'e Flores Conglomerate: insight into the Palaeogene to Early Miocene geodynamic evolution of Sardinia. Bull. Soc. Geol. Fr. 179, 51–72.

Di Vincenzo, G., Andriessen, P.A.M., Ghezzo, C., 1996. Evidence of Two Different Components in a Hercynian Peraluminous Cordierite-bearing Granite: the San Basilio Intrusion (Central Sardinia, Italy). J. Petrol. 37, 1175–1206.

Doe, B.R., 1997. Geochemistry of oceanic igneous rocks-ridges, islands, and arcs-with emphasis on manganese, scandium, and vanadium. Int. Geol. Rev. 39:1053–1112. https://doi.org/10.1080/00206819709465317.

Dostal, J., Dupuy, C., Carron, J.P., Le Guen de Kerneizon, M., Maury, R.C., 1983. Partition coefficients of trace elements: application to volcanic rocks of St. Vincent, West Indies. Geochim. Cosmochim. Acta 47:525–533. https://doi.org/10.1016/0016-7037(83)90275-2.

Ducea, M.N., Saleeby, J.B., 1996. Buoyancy sources for a large, unrooted mountain range, the Sierra Nevada, California: evidence from xenolith thermobarometry. J. Geophys. Res. Solid Earth 101 (B4), 8229–8244.

Dufek, J., Bachmann, O., 2010. Quantum magmatism: magmatic compositional gaps generated by melt-crystal dynamics. Geology 38, 687–690.

Duggen, S., Hoernle, K., van den Bogaard, P., Garbe-Schönberg, D., 2005. Post-collisional transition from subduction-to intraplate-type magmatism in the westernmost Mediterranean: evidence for continental-edge delamination of subcontinental lithosphere. J. Petrol. https://doi.org/10.1093/petrology/egi013.

Duke, J.M., 1976. Distribution of the period four transition elements among olivine, calcic clinopyroxene and mafic silicate liquid: experimental results. J. Petrol. 17:499–521. https://doi.org/10.1093/petrology/17.4.499.

Dungan, M.A., Davidson, J., 2004. Partial assimilative recycling of the mafic plutonic roots of arc volcanoes: an example from the Chilean Andes. Geology 32, 773–776.

Dunn, T., Sen, C., 1994. Mineral/matrix partition coefficients for orthopyroxene, plagioclase, and olivine in basaltic to andesitic systems: a combined analytical and experimental study. Geochim. Cosmochim. Acta 58:717–733. https://doi.org/10.1016/0016-7037(94)90501-0.

Dupuy, C., McNutt, R., Coulon, C., 1974. Détermination de Sr dans les andésites cénozoïques et les laves associées de Sardaigne Nord occidentale (Italie). Geochim. Cosmochim. Acta 38:1287–1296. https://doi.org/10.1016/0016-7037(74)90121-5.

Elsworth, D., Mattioli, G., Taron, J., Voight, B., Herd, R., 2008. Implications of magma transfer between multiple reservoirs on eruption cycling. Science 322, 246–248.

Foden, J.D., Green, D.H., 1992. Possible role of amphibole in the origin of andesite: some experimental and natural evidence. Contrib. Mineral. Petrol. 109:479–493. https://doi.org/10.1007/BF00306551.

Forsythe, L.M., Nielsen, R.L., Fisk, M.R., 1994. High-field-strength element partitioning between pyroxene and basaltic to dacitic magmas. Chem. Geol. 117:107–125. https://doi.org/10.1016/0009-2541(94)90124-4.

France, L., Ildefonse, B., Koepke, J., Bech, F., 2010. A new method to estimate the oxidation state of basaltic series from microprobe analyses. J. Volcanol. Geotherm. Res. 189: 340–346. https://doi.org/10.1016/j.jvolgeores.2009.11.023.

Franciosi, L., Lustrino, M., Melluso, L., Morra, V., D'Antonio, M., 2003. Geochemical characteristics and mantle sources of the Oligo-Miocene primitive basalts from Sardinia: the role of subduction components. Ofioliti 28, 105–114.

Franzini, M., Leoni, L., Saitta, M., 1972. A simple method to evaluate the matrix effects in X-ray fluorescence analysis. X-Ray Spectrom. 1:151–154. https://doi.org/10.1002/xrs.1300010406.

Frey, F.A., 1969. Rare earth abundances in a high-temperature peridotite intrusion. Geochimica et Cosmochimica Acta 33 (11):1429–1447. https://doi.org/10.1016/0016-7037(69)90183-5.

Frey, H.M., Lange, R.A., 2011. Phenocryst complexity in andesites and dacites from the Tequila volcanic field, Mexico: resolving the effects of degassing vs. magma mixing. Contrib. Mineral. Petrol. 162:415–445. https://doi.org/10.1007/s00410-010-0604-1.

Fujimaki, H., Tatsumoto, M., Aoki, K., 1984. Partition coefficients of Hf, Zr, and REE between phenocrysts and groundmasses. J. Geophys. Res. 89, B662–B672.

Green, T.H., Ringwood, A.E., 1968. Genesis of the calc-alkaline igneous rock suite. Contrib. Mineral. Petrol. 18, 105–162.

Green, T., Adam, J., Site, S., 1993. Proton microprobe determined trace element partition coefficients between pargasite, augite and silicate or carbonatitic melts. Am. Geophys. Union Trans. 74, 340.

Grove, T.L., Elkins-Tanton, L.T., Parman, S.W., Chatterjee, N., Müntener, O., Gaetani, G.A., 2003. Fractional crystallization and mantle-melting controls on calc-alkaline differentiation trends. Contrib. Mineral. Petrol. 145:515–533. https://doi.org/10.1007/s00410-003-0448-z.

Gudmundsson, A., 2011. Deflection of dykes into sills at discontinuities and magma-chamber formation. Tectonophysics 500, 50–64.

Gust, D.A., Perfit, M.R., 1987. Phase relations of a high-Mg basalt from the Aleutian Island Arc: implications for primary island arc basalts and high-Al basalts. Contrib. Mineral. Petrol. 97:7–18. https://doi.org/10.1007/BF00375210.

Holloway, J.R., Burnham, C.W., 1972. Melting relations of basalt with equilibrium water pressure less than total pressure. J. Petrol. 13:1–29. https://doi.org/10.1093/petrology/13.1.1.

Iain, S., Chassé, M., 2016. Scandium. In: White, William M. (Ed.), Encyclopedia of Geochemistry. 2016. Springer International Publishing, Switzerland:pp. 1–4. https://doi.org/10.1007/978–3–319-39193-9_281–1 (hal-01420736).

Iezzi, G., Mollo, S., Shahini, E., Cavallo, A., Scarlato, P., 2014. The cooling kinetics of plagioclase feldspar as revealed by electron-microprobe mapping. Am. Mineral. 99: 898–907. https://doi.org/10.2138/am.2014.4626.

Irving, A.J., Frey, F.A., 1984. Trace element abundances in megacrysts and their host basalts: constraints on partition coefficients and megacryst genesis. Geochim. Cosmochim. Acta 48:1201–1221. https://doi.org/10.1016/0016-7037(84)90056-5.

Jones, J.H., Drake, M.J., 1986. Geochemical constraints on core formation in the Earth. Nature 322:221–228. https://doi.org/10.1038/322221a0.

Klöck, W., Plame, H., 1988. Partitioning of siderophile and chalcophile elements between sulfide, olivine, and glass in a naturally reduced basalt from Disko Island, Greenland. Lunar Planeary Science Conference Proceedings. 18, pp. 471–483.

Larocque, J., Canil, D., 2010. The role of amphibole in the evolution of arc magmas and crust: the case from the Jurassic bonanza arc section, Vancouver Island, Canada. Contrib. Mineral. Petrol. 159:475–492. https://doi.org/10.1007/s00410-009-0436-z.

Le Bas, M.J., Le Maitre, R.W., Streckeisen, A., Zanettin, B., 1986. A chemical classification of volcanic rocks based on the total alkali silica diagram. J. Petrol. 27:745–750. https://doi.org/10.1093/petrology/27.3.745.

Leake, B.E., Woolley, A.R., Arps, C.E.S., Birch, W.D., Gilbert, M.C., Grice, J.D., Hawthorne, F.C., Kato, A., Kisch, H.J., Krivovichev, V.G., Linthout, K., Laird, J., Mandarino, J.A., Maresch, W.V., Nickel, E.H., Rock, N.M., Schumacher, J.C., Smith, D.C., Stephenson, N.C.N., Ungaretti, L., Whittaker, E.J.W., Youzhi, G., 1997. Nomenclature of amphiboles: report of the subcommittee on amphiboles of the International Mineralogical Association, commission on new minerals and mineral names. Can. Mineral. 35, 219–246.

Lecca, L., Lonis, R., Luxoro, S., Melis, E., Secchi, F., Brotzu, P., 1997. Oligo-Miocene volcanic sequences and rifting stages in Sardinia: a review. Period. Mineral. 66, 7–61.

Lewis, J.F., 1973. Petrology of ejected plutonic blocks of Soufriere volcano, St. Vincent, West Indies. J. Petrol. 14, 81–112.

Li, L., Xiong, X.L., Liu, X.C., 2017. Nb/Ta fractionation by amphibole in hydrous basaltic systems: implications for arc magma evolution and continental crust formation. J. Petrol. 15, egw070. https://doi.org/10.1093/petrology/egw070.

Lipman, P.W., Doe, B.R., Hedge, C.E., Steven, T.A., 1978. Petrologic evolution of the San Juan volcanic field, southwestern Colorado: Pb and Sr isotope evidence. Geol. Soc. Am. Bull. 89, 59–82.

Lonis, R., Morra, V., Lustrino, M., Melluso, L., Secchi, F., 1997. Plagioclase textures, mineralogy and petrology of tertiary orogenic volcanic rocks from Sindia (central Sardinia). Period. Mineral. 66, 185–210.

Luhr, J.F., Carmichael, I.S.E., 1980. The Colima Volcanic complex, Mexico. Contrib. Mineral. Petrol. 71:343–372. https://doi.org/10.1007/BF00374707.

Lustrino, M., Morra, V., Melluso, L., Brotzu, P., D'Amelio, F., Fedele, L., Franciosi, L., Lonis, R., Liebercknecht, A.M.P., 2004. The Cenozoic igneous activity of Sardinia. Period. Mineral. 73, 105–134.

Lustrino, M., Morra, V., Fedele, L., Franciosi, L., 2009. Beginning of the Apennine subduction system in central western Mediterranean: constraints from Cenozoic "orogenic" magmatic activity of Sardinia, Italy. Tectonics 28:1–23. https://doi.org/10.1029/2008TC002419.

Lustrino, M., Duggen, S., Rosenberg, C.L., 2011. The Central-Western Mediterranean: anomalous igneous activity in an anomalous collisional tectonic setting. Earth Sci. Rev. 104:1–40. https://doi.org/10.1016/j.earscirev.2010.08.002.

Lustrino, M., Fedele, L., Melluso, L., Morra, V., Ronga, F., Geldmacher, J., Duggen, S., Agostini, S., Cucciniello, C., Franciosi, L., Meisel, T., 2013. Origin and evolution of Cenozoic magmatism of Sardinia (Italy). A combined isotopic (Sr-Nd-Pb-O-Hf-Os) and petrological view. Lithos 180–181:138–158. https://doi.org/10.1016/j.lithos.2013.08.022.

Mattioli, M., Guerrera, F., Tramontana, M., Raffaelli, G., D'Atri, M., 2000. High-Mg tertiary basalts in Southern Sardinia (Italy). Earth Planet. Sci. Lett. 179:1–7. https://doi.org/10.1016/S0012-821X(00)00103-5.

McKay, G.A., Weill, D.F., 1976. Petrogenesis of KREEP. In: Merrill, R.B., Morris, R.V., Rhodes, J.M., Usselman, T.M. (Eds.), Proceedings of the 7th Lunar Science Conference: Petrogenetic Studies of Mare and Highland Rocks. Pergamon Press, New York, pp. 427–447.

McKay, G., Le, L., Wagstaff, J., Crozaz, G., 1994. Experimental partitioning of rare earth elements and strontium: constraints on petrogenesis and redox conditions during crystallization of Antarctic angrite Lewis Cliff 86010. Geochim. Cosmochim. Acta 58: 2911–2919. https://doi.org/10.1016/0016-7037(94)90124-4.

Melekhova, E., Blundy, J., Robertson, R., Humphreys, M.C.S., 2015. Experimental evidence for polybaric differentiation of primitive arc basalt beneath St. Vincent, Lesser Antilles. J. Petrol. 56:161–192. https://doi.org/10.1093/petrology/egu074.

Meurer, W.P., Claeson, D.T., 2002. Evolution of crystallizing interstitial liquid in an arc-related cumulate determined by LA ICP-MS mapping of a large amphibole oikocryst. J. Petrol. 43:607–629. https://doi.org/10.1093/petrology/43.4.607.

Morimoto, N., 1988. Nomenclature of pyroxenes. Mineral. Mag. 52, 535–550.

Molina, J.F., Moreno, J.A., Castro, A., Rodriguez, C., Fershtater, G.B., 2015. Calcic amphibole thermobarometry in metamorphic and igneous rocks: new calibrations based on plagioclase/amphibole Al-Si partitioning and amphibole/liquid Mg partitioning. Lithos 232, 286–305.

Mollo, S., Misiti, V., Scarlato, P., Soligo, M., 2012. The role of cooling rate in the origin of high temperature phases at the chilled margin of magmatic intrusions. Chem. Geol. 322–323:28–46. https://doi.org/10.1016/j.chemgeo.2012.05.029.

Mollo, S., Putirka, K., Misiti, V., Soligo, M., Scarlato, P., 2013. A new test for equilibrium based on clinopyroxene-melt pairs: clues on the solidification temperatures of Etnean alkaline melts at post-eruptive conditions. Chem. Geol. 352:92–100. https://doi.org/10.1016/j.chemgeo.2013.05.026.

Montigny, R., Edel, J.B., Thuizat, R., 1981. Oligo-Miocene rotation of Sardinia: K-Ar ages and paleomagnetic data of tertiary volcanics. Earth Planet. Sci. Lett. 54:261–271. https://doi.org/10.1016/0012-821X(81)90009-1.

Morra, V., Secchi, F.A., Assorgia, A., 1994. Petrogenetic significance of peralkaline rocks from Cenozoic calc-alkaline volcanism from SW Sardinia, Italy. Chem. Geol. 118: 109–142. https://doi.org/10.1016/0009-2541(94)90172-4.

Morra, V., Secchi, F.A.G., Melluso, L., Franciosi, L., 1997. High-Mg subduction-related tertiary basalts in Sardinia, Italy. Lithos 40:69–91. https://doi.org/10.1016/S0024-4937(96)00028-X.

Neave, D.A., Putirka, K.D., 2017. A new clinopyroxene-liquid barometer, and implications for magma storage pressures under Icelandic rift zones. Am. Mineral.

Nielsen, R.L., 1992. BIGD.FOR: a FORTRAN program to calculate trace-element partition coefficients for natural mafic and intermediate composition magmas. Comput. Geosci. 18:773–788. https://doi.org/10.1016/0098-3004(92)90024-L.

Oberti, R., Vannucci, R., Zanetti, A., Tiepolo, M., Brumm, R.C., 2000. A crystal chemical re-evaluation of amphibole/melt and amphibole/clinopyroxene DTi values in petrogenetic studies. Am. Mineral. 85:407–419. https://doi.org/10.2138/am-2000-0402.

Okamoto, K., 1979. Geochemical study on magmatic differentiation of Asama volcano, central Japan. J. Geol. Soc. Jpn. 85:525–535. https://doi.org/10.5575/geosoc.85.525.

Peccerillo, A., Taylor, S.R., 1976. Geochemistry of Eocene calc-alkaline volcanic rocks from the Katamonu area, northern Turkey. Contrib. Mineral. Petrol. 58, 63–81.

Pichavant, M., Macdonald, R., 2007. Crystallization of primitive basaltic magmas at crustal pressures and genesis of the calc-alkaline igneous suite: experimental evidence from St Vincent, lesser Antilles arc. Contrib. Mineral. Petrol. 154:535–558. https://doi.org/10.1007/s00410-007-0208-6.

Putirka, K.D., 2005. Igneous thermometers and barometers based on plagioclase + liquid equilibria: tests of some existing models and new calibrations. Am. Mineral. 90: 336–346. https://doi.org/10.2138/am.2005.1449.

Putirka, K.D., 2008. Thermometers and barometers for volcanic systems. Rev. Mineral. Geochem. 69:61–120. https://doi.org/10.2138/rmg.2008.69.3.

Putirka, K., Johnson, M., Kinzler, R., Longhi, J., Walker, D., 1996. Thermobarometry of mafic igneous rocks based on clinopyroxene-liquid equilibria, 0-30 kbar. Contrib. Mineral. Petrol. 123:92–108. https://doi.org/10.1007/s004100050145.

Putirka, K.D., Mikaelian, H., Ryerson, F., Shaw, H., 2003. New clinopyroxene-liquid thermobarometers for mafic, evolved, and volatile-bearing lava compositions, with applications to lavas from Tibet and the Snake River Plain, Idaho. Am. Mineral. 88: 1542–1554. https://doi.org/10.2138/am.2005.431.

Putirka, K.D., Perfit, M., Ryerson, F.J., Jackson, M.G., 2007. Ambient and excess mantle temperatures, olivine thermometry, and active vs. passive upwelling. Chem. Geol. 241: 177–206. https://doi.org/10.1016/j.chemgeo.2007.01.014.

Reid, F., 1983. Origin of the rhyolitic rocks of the Taupo volcanic zone, New Zealand. J. Volcanol. Geotherm. Res. 15:315–338. https://doi.org/10.1016/0377-0273(83)90105-1.

Ridolfi, F., Renzulli, A., 2012. Calcic amphiboles in calc-alkaline and alkaline magmas: Thermobarometric and chemometric empirical equations valid up to 1,130 °C and 2.2 GPa. Contrib. Mineral. Petrol. 163:877–895. https://doi.org/10.1007/s00410-011-0704-6.

Ridolfi, F., Renzulli, A., Puerini, M., 2010. Stability and chemical equilibrium of amphibole in calc-alkaline magmas: an overview, new thermobarometric formulations and application to subduction-related volcanoes. Contrib. Mineral. Petrol. 160:45–66. https://doi.org/10.1007/s00410-009-0465-7.

Roeder, P.L., Emslie, R.F., 1970. Olivine-liquid equilibrium. Contrib. Mineral. Petrol. 29: 275–289. https://doi.org/10.1007/BF00371276.

Ruprecht, W., Wörner, G., 2007. Variable regimes in magma systems documented in plagioclase zoning patterns: El Misti stratovolcano and Andahua monogenetic cones. J. Volcanol. Geotherm. Res. 165, 142–162.

Scarlato, P., Mollo, S., Del Bello, E., von Quadt, A., Brown, R.J., Gutierrez, E., Martinez-Hackert, B., Papale, P., 2017. The 2013 eruption of Chaparrastique volcano (El Salvador): effects of magma storage, mixing, and decompression. Chem. Geol. 448: 110–122. https://doi.org/10.1016/j.chemgeo.2016.11.015.

Shane, P., Smith, V.C., 2013. Using amphibole crystals to reconstruct magma storage temperatures and pressures for the post-caldera collapse volcanism at Okataina volcano. Lithos 156–159, 159–170.

Sisson, T.W., 1994. Hornblende-melt trace-element partitioning measured by ion microprobe. Chem. Geol. 117:331–344. https://doi.org/10.1016/0009-2541(94)90135-X.

Sisson, T.W., Grove, T.L., 1993. Experimental investigations of the role of H2O in calc-alkaline differentiation and subduction zone magmatism. Contrib. Mineral. Petrol. 113:143–166. https://doi.org/10.1007/BF00283225.

Skulski, T., Minarik, W., Watson, E.B., 1994. High-pressure experimental trace-element partitioning between clinopyroxene and basaltic melts. Chem. Geol. 117:127–147. https://doi.org/10.1016/0009-2541(94)90125-2.

Smith, D.J., 2014. Clinopyroxene precursors to amphibole sponge in arc crust. Nat. Commun. 5:4329. https://doi.org/10.1038/ncomms5329.

Spera, F.J., Bohrson, W.A., 2001. Energy-constrained open-system magmatic processes I: general model and energy-constrained assimilation and fractional crystallization (EC-AFC) formulation. J. Petrol. 42:999–1018. https://doi.org/10.1093/petrology/42.5.999.

Stamper, C.C., Blundy, J.D., Arculus, R.J., Melekhova, E., 2014. Petrology of plutonic xenoliths and volcanic rocks from Grenada, Lesser Antilles. J. Petrol. 55:1353–1387. https://doi.org/10.1093/petrology/egu027.

Streck, M.J., 2008. Mineral textures and zoning as evidence for open system processes. Rev. Mineral. Geochem. 69, 595–622.

Streck, M.J., Leeman, W.P., Chesley, J., 2007. High-magnesian andesite from Mount Shasta: a product of magma mixing and contamination, not a primitive mantle melt. Geology 35, 351–354.

Tilley, C.E., 1950. Some aspects of magmatic evolution. Q. J. Geol. Soc. Lond. 106, 37–61.

Tommasini, S., Poli, G., Halliday, A.N., 1995. The role of sediment subduction and crustal growth in Hercynian plutonism: isotopic and trace element evidence from the Sardinia-Corsica batholith. J. Petrol. 36:1305–1332. https://doi.org/10.1093/petrology/36.5.1305.

Turner, S.J., Izbekov, P., Langmuir, C., 2013. The magma plumbing system of Bezymianny Volcano: insights from a 54 year time series of trace element whole-rock geochemistry and amphibole compositions. J. Volcanol. Geotherm. Res. 263, 108–121.

Ushioda, M., Takahashi, E., Hamada, M., Suzuki, T., 2014. Water content in arc basaltic magma in the Northeast Japan and Izu arcs: an estimate from Ca/Na partitioning between plagioclase and melt. Earth Planets Space 66:1–10. https://doi.org/10.1186/1880-5981-66-127.

Villemant, B., Jaffrezic, H., Joron, J.L., Treuil, M., 1981. Distribution coefficients of major and trace-elements - fractional crystallization in the alkali basalt series of Chaine-des-Puys (Massif Central, France). Geochim. Cosmochim. Acta 45, 1997–2016.

Yamamoto, M., 1984. Origine of calc-alkaline andesite from Oshima-Oshima volcano, north Japan. Journal of the Faculty of Science, Hokkaido University. Series 4. Geol. Mineral. 21, 77–131.